Lactylation-based machine algorithm combined with multi-omics analysis to predict prognosis in cervical cancer

RUYUE WANG[1,2], LI NING[1,2], XIU LI[1,2], YATING XU[1,2], YU SI[1,2], HONGTING ZHAO[2] and QINGLING REN[1,2]

[1]Department of Gynecology, Affiliated Hospital of Nanjing University of Chinese Medicine, Nanjing, Jiangsu 210029, P.R. China; [2]Department of Gynecology, The Chinese Clinical Medicine Innovation Center of Obstetrics, Gynecology and Reproduction in Jiangsu Province, Nanjing, Jiangsu 210004, P.R. China

Received July 15, 2025; Accepted November 25, 2025

DOI: 10.3892/ol.2026.15486

Abstract. Although lactylation has been investigated in cancer biology, its mechanistic role in cervical cancer remains unclear. This study integrated RNA-sequencing data from TCGA, three GEO datasets, and single-cell data (GSE44001) to identify lactylation-associated genes (LAGs) involved in cervical cancer. Differential expression analysis, WGCNA, and lactylation-related gene sets were combined to identify candidate genes. Multiple machine learning algorithms were employed to construct a prognostic model, which was further validated using Cox regression, receiver operating characteristic analysis, immune infiltration profiling, functional enrichment, and cell-cell communication analysis. A total of 43 overlapping co-expressed genes were identified, and 14 LAGs strongly associated with prognosis were incorporated into a risk-scoring system. The model demonstrated robust predictive performance and enrichment in pathways associated with carbon metabolism and glycolysis, with notable immune differences between risk groups, particularly in mast cells and neutrophils. Drug sensitivity analysis showed positive correlations between the risk score and IC_{50} values of paclitaxel and rapamycin, and a negative correlation with midostaurin. Mendelian randomization revealed a causal association between HMGN1 and cervical cancer risk. *In vitro* assays demonstrated that HMGN1 inhibition significantly suppressed SiHa and HeLa cell proliferation and induced S-phase arrest, highlighting its potential as a therapeutic target. In conclusion, this study developed a reliable LAG-based prognostic model and uncovered key lactylation-related mechanisms in cervical cancer, providing new insights for biomarker discovery and personalized therapeutic strategies.

Correspondence to: Professor Qingling Ren, Department of Gynecology, Affiliated Hospital of Nanjing University of Chinese Medicine, 155 Hanzhong Road, Qinhuai, Nanjing, Jiangsu 210029, P.R. China
E-mail: yfy0047@njucm.edu.cn

Key words: lactoylation, cervix, immunotherapy, prognostic model, multi-omics, Mendelian randomization

Introduction

Cervical cancer remains one of the leading causes of cancer-related mortalities among women, ranking fourth in both incidence and mortality rates for malignancies in women globally (1,2). Cervical cancer accounts for ~9% of novel cancer cases worldwide and 8% of all cancer mortalities (3). Current prevention strategies primarily rely on vaccination and molecular screening programs (4). However, large-scale vaccine implementation remains constrained by socioeconomic disparities and uneven human development levels, hindering universal coverage (5). Standard treatments for cervical cancer include surgery, radiotherapy and platinum-based chemotherapy. In recent years, stimulus-responsive hydrogel therapy and 5-aminolevulinic acid photodynamic therapy (5-ALA-PDT) have emerged as promising systemic therapeutic options (6-8). Notably, the application of immune checkpoint inhibitors has markedly improved survival outcomes for advanced-stage patients (9). Despite these advances, there remains an urgent need to identify more reliable biomarkers to potentially guide the development of novel targeted therapeutic strategies in the future.

Cancer is characterized by somatic genomic instability and metabolic reprogramming of cancer cells serves a key role in driving tumorigenesis (10). Metabolic enzymes and their accumulated metabolites often serve as substrates for post-translational modifications-such as lactylation, acetylation and succinylation-which in turn induce epigenetic remodeling and influence cancer progression (11,12). The extracellular matrix (ECM), a key component of the tumor microenvironment (TME), can be remodeled by metabolic byproducts such as lactate. These substances promote tumor cell invasion and metastasis by altering cellular metabolic states (13). This metabolic adaptation mechanism enables tumor cells to meet the energy and biosynthetic demands required for sustained growth and proliferation (14). Recently, lactylation has emerged as a novel post-translational modification with notable implications in cancer biology. Previous studies revealed that abnormal protein lactylation in multiple malignancies, including breast (15), gastric (16) and non-small cell lung cancer (17), suggesting that dysregulation of lactylation pathways may promote tumor progression and constitute potential therapeutic targets in the future (11).

The present study comprehensively investigated the role of lactylation-associated genes (LAGs) in cervical cancer by integrating multi-omics data from The Cancer Genome Atlas (TCGA) and the Gene Expression Omnibus (GEO) alongside single-cell transcriptomics analysis. Candidate LAGs were screened using single-cell RNA-sequencing (scRNA-seq) data and a prognostic model was constructed using multiple machine learning algorithms in combination with GEO datasets. The predictive efficacy of the LAGs-based model for cervical squamous cell carcinoma (CESC) was systematically evaluated. Functional enrichment analysis explored biological relevance, immune microenvironment associations and intercellular communication patterns. Furthermore, Mendelian randomization (MR) analysis was employed to assess the causal relationship between key prognostic LAGs and cervical cancer risk. Lastly, *in vitro* experiments using SiHa and HeLa cell lines validated the role of high-mobility group nucleosome-binding protein 1 (HMGN1) in cervical cancer cell proliferation and progression. Collectively, these findings provide novel insights for cervical cancer prognosis assessment and pave potential pathways for personalized therapeutic interventions in the future. The overall study design is illustrated in Fig. 1.

Materials and methods

Data collection and processing. The TCGA-CESC dataset (accessed December 20, 2024) contains 306 CC tumor tissues and survival data from 293 samples. (https://portal.gdc.cancer.gov/) (18). Samples with incomplete or missing clinicopathological information were excluded. Differential gene expression analysis was performed using the R package 'limma' (version 3.64.3) (19). All datasets were downloaded from the GEO database (https://www.ncbi.nlm.nih.gov/geo/), including three microarray datasets [GSE122697 (20), GSE146114 (21) and GSE63514 (22)] for WGCNA analysis, the scRNA-seq dataset GSE44001 (23) and the validation set GSE30760 (24). The GSE7803 (25) dataset was used for independent external validation of the prognostic model. At present, no other publicly available scRNA-sequencing datasets with sufficient sample size, annotation quality and relevance to cervical cancer are available; therefore, GSE44001 was selected as the only suitable dataset for single-cell analysis in the present study. Detailed information about the datasets is provided in Table SI. Batch effects were mitigated using the 'sva' package (version 3.56.0) (26). Furthermore, 325 LAGs were collected from previously published studies, as detailed in Table SII (27-29).

To further assess the association between the prediction model and the immune response of the patients, the present study integrated data from the IMvigor210 cohort using the 'IMvigor210CoreBiologies' R package (version 1.15.0.) (30). The present study also obtained cervical cancer genome-wide association studies (GWAS) data and LAG expression quantitative trait loci (eQTL) GWAS data from the FinnGen database (https://risteys.finngen.fi/) for MR analysis (31). The cervical cancer GWAS dataset, 'FinnGen R12 CD2 INSITU CERVIX UTERI EXALLC' contains data on 20,104,836 single nucleotide polymorphisms (SNPs).

Single-cell transcriptome data analysis and processing. scRNA-seq data from both normal and cervical cancer tissues were obtained from the GSE168652 dataset. Data preprocessing and quality control were performed using the 'Seurat' R package (version 5.3.1; https://satijalab.org/seurat/) (32). Cells with low gene counts or high mitochondrial gene percentages were filtered out to ensure data integrity. Batch effects across samples were corrected using the 'Harmony' package (version 1.2.4; https://github.com/immunogenomics/harmony) (33). Following normalization and scaling, unsupervised cell clustering was performed at a resolution of 0.8 and dimensionality reduction was visualized using t-distributed stochastic neighbor embedding. To assess the activity of lactylation-related gene sets in individual cells, the 'AddModuleScore' function in Seurat was applied. In addition, intercellular communication networks were analyzed using the 'CellChat' R package to explore signaling interactions among different cell populations (version 2.2.0; https://github.com/jinworks/CellChat) (34).

Differential gene expression analysis and WGCNA construction. Differentially expressed genes (DEGs) were identified using three GEO datasets: GSE122697, GSE146114 and GSE63514. These datasets were chosen for their high-quality, well-annotated expression profiles and adequate sample sizes, ensuring data reliability and reproducibility. The grouping details for each dataset are provided in Table SI. To minimize batch effects, the ComBat function from the 'sva' R package was applied (version 3.22) (26). Subsequently, a disease-specific co-expression network was constructed using the 'WGCNA' R package (version 1.73) (35). The optimal soft-thresholding power (β) was selected to ensure scale-free topology and modules most correlated with cervical cancer were identified for downstream analyses.

Construction of LAGs-related prognostic model. The highly disease-associated genes identified by WGCNA were cross-analyzed with differentially expressed genes and lactation-related genes to identify potential LAG-associated prognostic candidate genes. Subsequently, these genes were subjected to feature selection and prognostic modeling using multiple machine learning algorithms, including least absolute shrinkage and selection operator (LASSO) (36), Stepwise Cox (Backward), CoxBoost (37), random survival forest (RSF) (38), generalized boosted regression model and survival support vector machine (18-21). Each algorithm was independently evaluated for the prognostic performance of the candidate genes in TCGA training cohort and GSE30760 validation cohort. The concordance index (C-index) was used to quantify model performance and the models were ranked according to their average C-index values. The StepCox (Backward) model achieved the highest predictive performance [area under the curve (AUC)=0.82; C-index=0.79], outperforming CoxBoost and survival SVM while maintaining simplicity and interpretability. To minimize overfitting and ensure robustness, the StepCox (Backward) model was lastly selected for downstream analysis, which is consistent with previous studies demonstrating the stability and strong generalization ability of this model in cancer prognosis modeling (39).

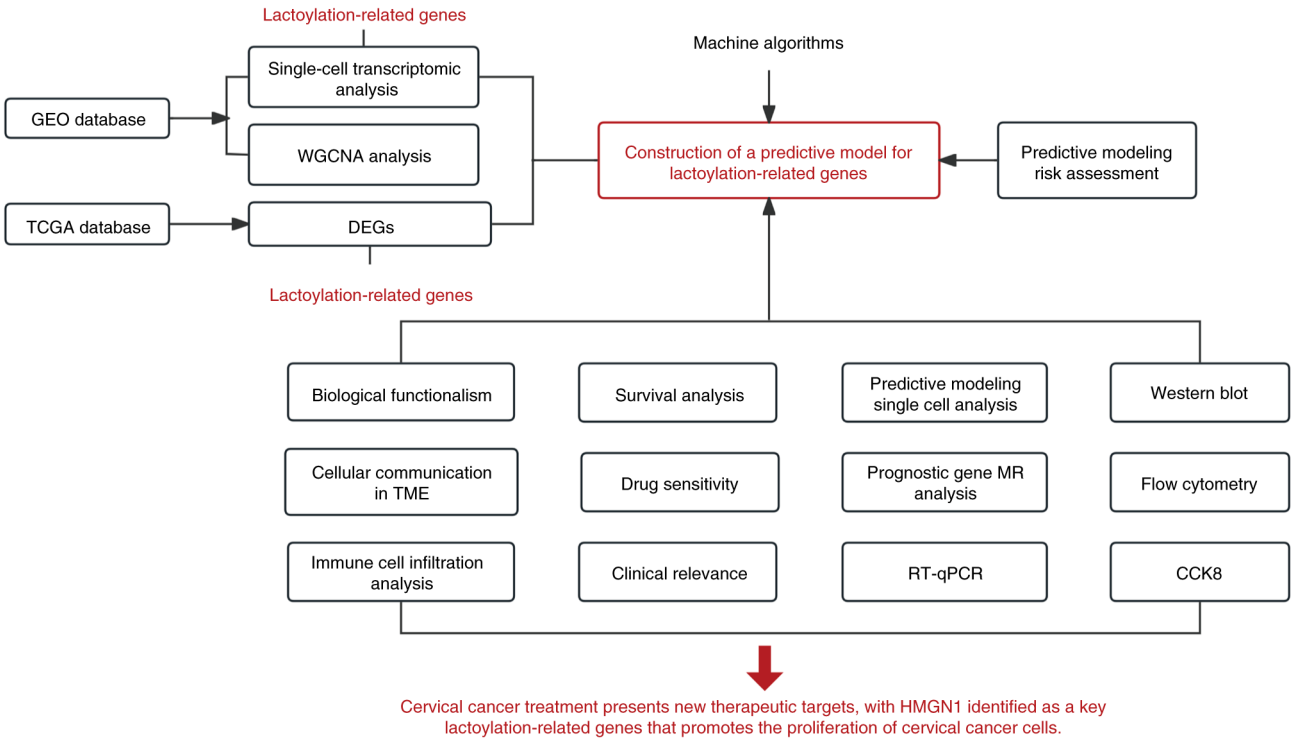

Figure 1. Framework diagram. WCGNA, weighted gene co-expression network analysis; DEGs, differentially expressed genes; TCGA, The Cancer Genome Atlas; GEO, Gene Expression Omnibus; RT-qPCR, reverse transcription-quantitative PCR; CCK-8, Cell Counting Kit-8; TME, tumor microenvironment; MR, Mendelian randomization; HMGN1, high-mobility group nucleosome-binding protein 1.

Evaluation of predictive model performance and independent prognostic analysis. After obtaining the LAGs risk score of each patient, patients were divided into high-risk and low-risk groups based on the median of the LAGs risk score distribution within the cohort. Survival outcomes, including progression-free survival (PFS), disease-specific survival (DSS) and disease-free interval (DFI), were compared between the two groups using Kaplan-Meier analysis implemented in the 'survminer' R package (version 0.5.1; https://rpkgs.datanovia.com/survminer/index.html). The predictive accuracy of the model was further assessed by calculating the AUC for 1-, 3- and 5-year overall survival (OS) using the 'timeROC' R package (version 0.4) (40). Differences in risk scores across clinical subgroups, such as tumor (T), lymph node (N) and metastasis (M) stage and histological grade (41), were examined using TCGA-CESC clinical data. To determine whether the LAGs-based risk model serves as an independent prognostic factor, univariate and multivariate Cox regression analyses were performed. Lastly, a nomogram integrating the LAGs risk score and key clinical variables was constructed to predict individual patient survival probabilities and enhance the model's clinical applicability. Simultaneously, the GEPIA2.0 database (http://gepia2.cancer-pku.cn/) (42) was used to validate the survival analysis.

Functional enrichment analysis of the LAGs-based risk model. To explore the biological pathways underlying differences between the high- and low-risk groups, Gene Set Enrichment Analysis (GSEA) was performed (43). Additionally, enrichment scores were quantified at the individual sample level using single-sample gene set enrichment analysis (ssGSEA) implemented in the R package GSVA (version 2.2.1) on the TCGA-CESC (Cervical squamous cell carcinoma and endocervical adenocarcinoma) dataset downloaded from The Cancer Genome Atlas (TCGA) via the GDC Data Portal, to assess pathway activity (44). Functional annotations were further investigated using Gene Ontology (GO) and Kyoto Encyclopedia of Genes and Genomes (KEGG) enrichment analyses to identify biological processes and signaling pathways associated with the LAGs risk model. Pathways with $P<0.05$ were considered statistically significant.

Immune landscape characterization. To examine immune infiltration patterns across LAGs risk subgroups, the ESTIMATE analysis was performed to determine the malignant tumor stroma and immune cell (ESTIMATE) scores of patients (version 4.7.0) (45). The CIBERSORT algorithm (https://cibersortx.stanford.edu/) was then used to estimate the relative abundance of immune cell populations, while ssGSEA was applied to assess immune cell signature enrichment and immune-related functions. Concurrently, ssGSEA was applied to assess the enrichment of immune cell signatures and immune-related functions. Statistical differences between subgroups were evaluated using the Wilcoxon rank-sum test. In addition, to assess intratumoral heterogeneity, the Mutant-Allele Tumor Heterogeneity (MATH) algorithm was utilized to calculate mutation-derived heterogeneity scores (version 2.4.6) (46). These MATH scores were subsequently incorporated into survival analyses to examine their association with patient prognosis and genomic instability.

Drug sensitivity analysis of LAGs risk subgroups. To evaluate potential therapeutic implications of the LAGs-based risk model, drug response prediction was performed using the 'pRRophetic' R package (version 0.5.1) (47). The half-maximal inhibitory concentration (IC_{50}) values of commonly used chemotherapeutic and targeted agents were estimated for each patient. Differences in predicted drug sensitivity between high- and low-risk groups were compared using the Wilcoxon rank-sum test, with $P<0.05$ considered statistically significant. These analyses aimed to identify potential compounds with differential efficacy across risk subgroups, providing a foundation for personalized treatment strategies in CESC.

Two-sample MR analysis of cervical cancer and LAGs prediction models. To further elucidate the causal relationship between LAGs prediction models and cervical cancer, two-sample MR analysis was employed to assess whether the expression levels of prognostic LAGs exert a causal effect on cervical cancer susceptibility. SNPs were selected as instrumental variables (IVs) if they demonstrated significant association with the exposure variable ($P<5x10^{-8}$). To ensure variant independence and minimize linkage disequilibrium (LD) effects, SNPs were clustered using an LD threshold of $R^2<0.001$ and a 10,000 kb clustering window. Variants with minor allele frequency <0.01 or F-statistic <10 were excluded to avoid weak instrument bias. The inverse variance weighting (IVW) method was employed as the primary analysis to estimate causal effects between LAGs and cervical cancer. Heterogeneity among IVs was assessed using the Cochran Q test, while potential horizontal pleiotropy and directional bias were assessed via MR-Egger regression. Sensitivity analyses, including stepwise exclusion tests, validated the robustness of causal estimates. All MR analyses were performed using the 'TwoSampleMR' and 'MRPRESSO' R packages (version 1.0) (48,49). Sensitivity analyses were conducted for the two-sample MR studies, including leave-one-out tests, pleiotropy analysis via the MR-Egger intercept test and heterogeneity analysis using Cochran's Q test (50). These analyses ensure the robustness and validity of the MR findings by identifying potential biases or heterogeneity in the genetic instruments used. Final causal estimates were visualized with forest plots and scatterplots to display the direction and magnitude of the association.

Cell culture and transfection. Human cervical squamous cell carcinoma cell lines SiHa (cat. no. HTB-35) and HeLa (cat. no. CRM-CCL-2) were obtained from the American Type Culture Collection and the human keratinocyte cell line HaCaT was obtained from The Cell Bank of Type Culture Collection of the Chinese Academy of Sciences (SCSP-5091; Beijing, China). Although short tandem repeat analysis was not performed, the HaCaT cells were purchased from a certified national cell bank with traceable origins and their authenticity was confirmed by morphological observation and mycoplasma testing. All cell lines were cultured in DMEM (cat. no. KGL1201-500; Jiangsu KeyGen Biotech Co., Ltd.) containing 10% FBS (cat. no. C04001-500; Shanghai Xiaopeng Biotechnology Co., Ltd.) and 1% penicillin-streptomycin-amphotericin B (cat. no. P7630; Beijing Solare Technology Co., Ltd.) at 37˚C in a humidified incubator with 5% CO_2.

SiHa and HeLa cells were seeded into 6-well plates and transfected with HMGN1-specific small interfering RNA (siRNA) or non-targeting control (NC) siRNA using siTran 2.0™ (cat. no. TT320002; Origene Technologies, Inc.) according to the manufacturer's instructions. The sequences and catalog numbers of the HMGN1-specific siRNAs and NC siRNA are provided in Table SIII (Tsigke). Cells were cultured to approximately 60-70% confluence prior to transfection. A final concentration of 50 nM siRNA was used for each transfection. For each well of a 6-well plate, the appropriate amount of siRNA was gently mixed with 2.4 μl siTran 2.0™ reagent and 100 μl transfection buffer, followed by incubation at room temperature for 15 min to allow complex formation. The complexes were then added dropwise to the cell culture medium. After incubating the cells at 37˚C for 12 h, the medium was replaced with fresh growth medium. Cells were collected after an additional 12 or 24 h incubation. RNA and proteins were extracted separately for subsequent analysis.

RNA extraction and reverse transcription-quantitative PCR (RT-qPCR). Total RNA was extracted from SiHa and HeLa cells using the RNeasy™ Kit (cat no. R0027; Beyotime Biotechnology) according to the manufacturer's instructions. The extracted total RNA was then reverse transcribed into complementary DNA (cDNA) using SuperMix (R323-01; Vazyme Biotech Co., Ltd.). After cDNA synthesis, qPCR was performed on QuantStudio 5 instrumentation using SYBR® Green PCR Master Mix (cat. no. Q311-02; Vazyme Biotech Co., Ltd.). The thermocycling conditions were as follows: An initial pre-denaturation at 95˚C for 10 min, followed by 40 cycles of denaturation at 95˚C for 10 sec, annealing at 58˚C for 30 sec and extension at 72˚C for 30 sec. GAPDH was used as the internal reference gene for normalization. Relative gene expression levels were calculated using the $2^{-\Delta\Delta Cq}$ method (51). The human-derived mRNA sequences of the 14 genes for the lactylation prediction model are shown in Table SIV. All mRNA sequences were provided by Beijing Qingke Biotechnology Co., Ltd.

Western blotting analysis. Cells were collected and the medium was discarded. Total protein was extracted using RIPA lysis buffer (cat no. P0013B; Beyotime Biotechnology) supplemented with protease and phosphatase inhibitors (cat no. P1045; Beyotime Biotechnology). Samples were centrifuged at 12,000 x g for 15 min at 4˚C and the supernatant was collected for subsequent analysis. Protein concentration was quantified using the BCA Protein Assay Kit (cat no. 20201ES86, Shanghai Yeasen Biotechnology Co., Ltd). Equal amounts (10 μg) of protein were separated by 10% SDS-PAGE and transferred onto PVDF membranes (cat no. IPVH00010; MerckKGaA). Membranes were incubated in Rapid Blocking Buffer (cat. no. P30500; Suzhou Xinsaimai Biotechnology Co., Ltd.) for 20 min at room temperature to minimize non-specific binding. After blocking, membranes were incubated overnight at 4˚C with anti-HMGN1 (1:1,000; cat no. PK87656; Abmart, Inc.) and anti-β-actin (1:1,000; cat no. A17910; ABclonal, Inc.; internal control). After washing with 0.1% TBS-Tween, membranes were incubated with HRP-conjugated anti-rabbit secondary antibody (cat. no. ZB-2306; ZSGB-Bio, Inc.) for 1 h at room temperature. The membranes were detected using

an ultra-sensitive ECL kit (cat no. P10100; Suzhou CellPro Biotechnology Co., Ltd.) and quantified using ImageJ software (version 1.0; National Institutes of Health).

Cell Counting Kit-8 (CCK-8) assay. Cell proliferation was assessed using the CCK-8 Assay Kit (cat. no. C0005; TargetMol Chemicals Inc.). Cells were seeded in 96-well plates and absorbance was measured at 24, 48 and 72 h after adhesion. To assess cell proliferation, 10 μl of CCK-8 reagent was added to each well and the cells were then incubated at 37˚C and 5% CO_2 for 1 h. The absorbance at 450 nm was then measured using a microplate reader to determine cell viability.

Flow cytometry analysis. Cell cycle distribution was analyzed using propidium iodide (PI) staining. Transfected SiHa and HeLa cells were seeded into 6-well plates and cultured under standard conditions. Cells were collected, washed twice with PBS (cat. no. C0221A; Beyotime Biotechnology) and fixed in pre-cooled 70% ethanol (cat. no. Y263010; Beyotime Biotechnology) at 4˚C for 8 h. Fixed cells were centrifuged, washed and resuspended in staining buffer containing RNase A (cat. no. ST576; Beyotime Biotechnology) and 5 μg/ml PI (cat. no. G1021; Wuhan Servicebio Technology Co. Ltd.). After incubation for 20 min in the dark at room temperature, samples were analyzed using a FACSCalibur flow cytometer (BD Biosciences) and data were processed with CytExpert 2.0 software (Becton; Dickinson and Company).

Statistical analysis. All statistical analyses were conducted using R software (version 4.4.1; Posit Software, PBC) and GraphPad Prism (version 10.6.1; Dotmatics). All results represent the mean ± standard deviation of at least three independent experiments. Intergroup comparisons were performed using the two-tailed unpaired Student's t-test, while comparisons among multiple groups employed one-way ANOVA followed by Tukey's post hoc test. The relationship between two continuous variables was assessed using Wilcoxon rank-sum. To compare differences in Kaplan-Meier survival curves, the two-tailed log-rank test was applied. $P<0.05$ was considered to indicate a statistically significant difference, unless otherwise specified.

Results

Integration of single-cell transcriptomics and WGCNA identifies LAGs. The GSE44001 dataset, comprising transcriptomic data from 300 patients with cervical cancer, included scRNA-seq data for a total of 22,702 cells. After rigorous quality control and filtering, cells were categorized into eight major clusters: Columnar and squamous epithelial cells, $CD8^+$ T cells, $CD4^+$ T cells, stromal cells, cancer cells, basal blood cells, and endothelial cells (Fig. 2A). The proportions of these cell populations are shown in a bar chart (Fig. 2B). To evaluate the activity of LAGs across different cell types, the 'AddModuleScore' function of the 'Seurat' package was applied. The resulting scores demonstrated that squamous and columnar epithelial cells exhibited higher LAG activity compared with other clusters (Fig. 2C and D), suggesting that LAGs play a key role in cervical cancer pathogenesis, as these epithelial cells are involved in tumor initiation and progression. Elevated LAG levels in these cells may be associated with their influence on cervical cancer progression. Based on the distribution of LAG activity, cells were stratified into high- and low-LAG groups, yielding 5,443 DEGs for subsequent analysis. To validate these findings, three GEO datasets (GSE122697, GSE146114 and GSE63514) were integrated after batch correction using the ComBat algorithm (Fig. S1A-D). From these datasets, disease-related DEGs were identified and the top 50 genes were visualized in a heatmap (Fig. 2E).

Next, WGCNA was performed to identify gene modules associated with cervical cancer. After removing outlier samples, hierarchical clustering and correlation analyses between normal and tumor groups were performed using the ssGSEA algorithm. With a merging threshold of 0.25, a total of nine co-expression modules were identified (Fig. 2F and G). Among them, the turquoise module (MEturquoise) revealed the strongest positive correlation with cervical cancer progression ($r=0.57$; $P<0.001$). The strong association between gene significance and module membership within this module ($r=0.96$; $P<0.001$; Fig. 2H) further confirmed its biological relevance. Genes within the turquoise module were thus selected for further analysis. Differential expression analysis between tumor and normal tissues revealed significant gene expression changes (adjusted $P<0.05$; $\log_2FC>0.5$), which were visualized in a volcano plot (Fig. 2I). By intersecting turquoise module genes, DEGs and LAGs, a total of 43 overlapping genes were identified as LAGs (Fig. 2J). GO enrichment analysis revealed that these LAGs were predominantly involved in 'monosaccharide metabolic process', 'hexose metabolic process' and 'pyridine-containing compound metabolic process'. They were also enriched in cellular components such as the 'nuclear envelope' and 'cell-substrate junction' and exhibited molecular functions associated with 'tubulin binding' (Fig. 2K; Table SV).

Construction and validation of a prognostic model based on CESC-related LAGs. To elucidate the prognostic relevance of LAGs in CESC, multiple machine learning algorithms were employed to construct and evaluate prognostic models based on 43 differentially expressed LAGs identified in prior analyses. TCGA-CESC cohort was used as the training dataset, whereas GSE30760 served as the independent validation cohort. A total of 101 predictive models were generated via cross-validation and their predictive efficacy was systematically compared using the C-index across both training and validation datasets (Fig. 3A). After excluding models exhibiting overfitting tendencies, the StepCox (Backward) model demonstrated the most stable and robust performance and was therefore selected as the optimal prognostic model. This refined model incorporated 14 feature genes with significant prognostic relevance. For each patient, a risk score was calculated by summing the expression levels of these 14 genes weighted by their respective Cox regression coefficients (Fig. 3B). Based on the median risk score, patients were stratified into high-risk and low-risk groups. Kaplan-Meier survival analysis revealed that patients in the high-risk group exhibited significantly worse OS compared with those in the low-risk group ($P<0.001$; Fig. 3C). Consistent findings were observed for DSS and PFI, with low-risk patients demonstrating notably increased clinical outcomes ($P<0.0001$; Fig. 3D and E). To

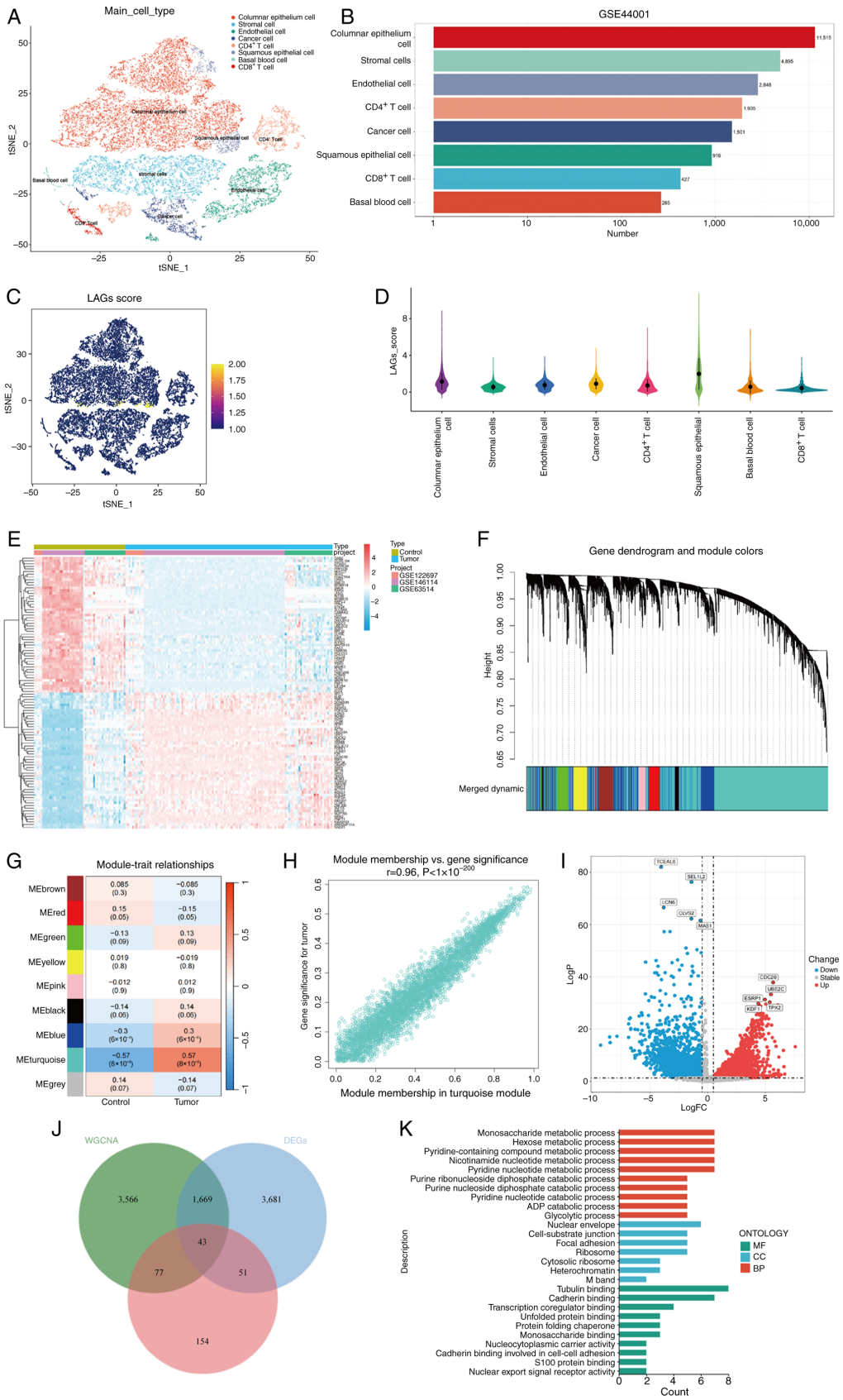

Figure 2. Single-cell transcriptome combined with Weighted Gene Co-expression Network Analysis to assess lactation-associated genes. (A) t-SNE plot depicts cell type identification based on marker genes. (B) Bar graph displays the distribution of cells in eight cell types. (C) Activity scores of lactoylation-associated genes (LAGs). (D) Distribution of LAGS scores in different cell types. (E) Heat map indicates differential gene expression between normal and tumor samples in Gene Expression Omnibus dataset. (F) Hierarchical clustering of genes into different modules, each represented by a different color. (G) Heat map indicates the correlation between gene modules and disease states. (H) Scatter plot depicts the relationship between turquoise module genes and module members. (I) The volcano plot displays differential expression of turquoise module genes. (J) The Venn diagram presents the overlap of turquoise module genes, DEGs and lactylation-associated genes. (K) Gene Ontology enrichment analysis of lactylation-associated genes. t-SNE, t-distributed stochastic neighbor embedding; LAGs, lactylation-associated genes; DEGs, differentially expressed genes; MF, molecular function; BP, biological process; CC, cellular component.

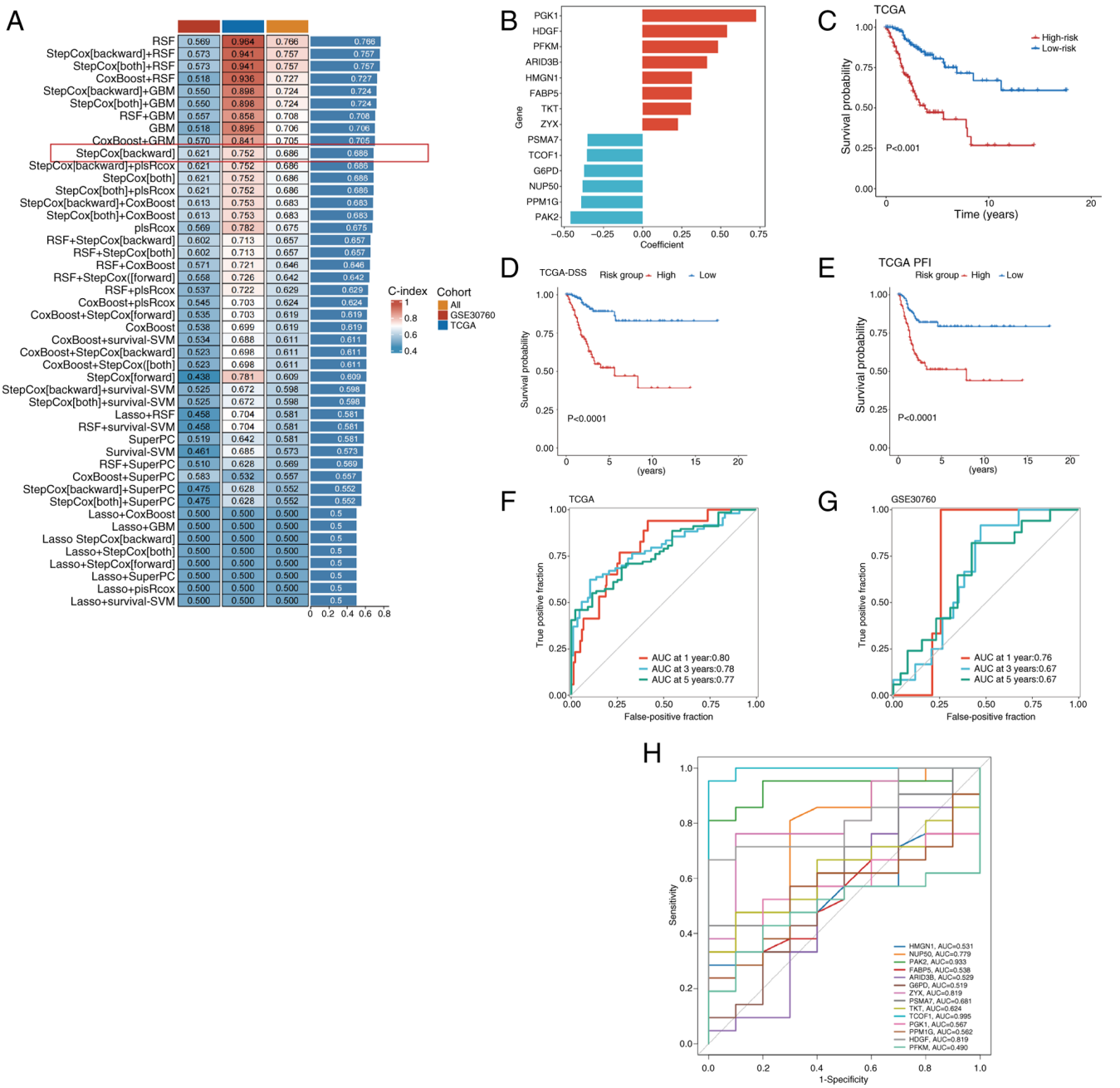

Figure 3. Characterized LAG genes were screened using machine algorithms. (A) Develop predictive models using the 10-fold cross-validation method and calculate the C-index for each model for the training and validation data sets. (B) Bar graph depicting regression coefficients for 14 genes determined by Cox regression analysis. (C) Kaplan-Meier curves demonstrating the risk score and overall survival of patients in TCGA-CESC cohort. Kaplan-Meier curves for (D) DSS and (E) PFI. ROC curves of the LAGs prognostic model at 1, 3 and 5 years in (F) TCGA training set and (G) GSE30760 validation set. (H) ROC curves indicating the AUC values of 14 prognostic genes in the GSE7803 dataset. LAGs, lactylation-associated genes; C-index, concordance-index; TCGA, The Cancer Genome Atlas; DSS, disease-specific survival; PFI, progression-free interval; CESC, cervical squamous cell carcinoma; AUC, area under the curve; ROC, receiver operating characteristic; HMGN1, high-mobility group nucleosome-binding protein 1; TKT, transketolase; ZYX, zyxin; PAK2, p21 (RAC1) activated kinase 2; ARID3B, AT-rich interaction domain 3B; FABP5, fatty acid binding protein 5; HDGF, hepatoma-derived growth factor.

further assess the discriminatory capability of the model, time-dependent receiver operating characteristic (ROC) curve analyses were conducted. In TCGA training cohort, the model achieved AUC values of 0.80, 0.78 and 0.77 for 1-, 3- and 5-year survival, respectively (Fig. 3F). Similar results were obtained in the GSE30760 validation cohort, yielding AUC values of 0.76, 0.67 and 0.67, indicating moderate generalization ability and demonstrating the acceptable performance of the model in short-term survival prediction (Fig. 3G). Furthermore, external validation using the GSE7803 dataset further confirmed the predictive reliability of the 14-gene model, with AUC values >0.5 for all included genes except PFKM. However, due to sample limitations, the predictive capability of genes other than PAK2 and TCOF1 may be limited (Fig. 3H). These findings indicate that LAG-based predictive models may be able to evaluate the prognosis of patients with cervical cancer and provide important reference for clinical stratification management.

Clinical prognostic stratification and independent prognostic analysis of the LAGs-based model. To further evaluate the clinical applicability and prognostic independence of the LAGs risk model in cervical cancer, the present study examined the relationship between the LAGs-derived risk score and diverse clinicopathological characteristics using stratified and Cox regression analyses. This comprehensive evaluation aimed to assess the ability of the model to predict patient outcomes across different clinical subgroups. Patients were stratified according to clinical parameters, including age (>60 vs. ≤60 years), T stage (T1; T2; T3 and T4), N stage (N0, N1 and NX), M stage (M0, M1 and MX) and tumor stage (I; II; III and IV), as illustrated in the clinical distribution plot (Fig. 4A and B). Notably, patients in the stage M1, III-IV and T3-4 subgroups exhibited significantly higher risk scores compared with those patients in the M0, I-II and T1-2 subgroups, respectively (Fig. 4C and D). These findings indicate a strong association between elevated LAGs risk scores and advanced tumor stage as well as unfavorable prognosis in CESC.

ROC curve analysis further confirmed the predictive utility of the LAGs-based model, with an AUC value of 0.76 in distinguishing the prognosis of patients with different M stages, indicating moderate predictive capability (Fig. 4E). In addition, stratified analyses by age and tumor stage demonstrated that high-risk patients consistently exhibited worse survival outcomes (Fig. 4F). Kaplan-Meier analyses of the 14 model genes using the GEPIA2 database that low expression levels of transketolase (TKT) and phosphoglycerate kinase 1 (PGK1) were significantly associated with improved prognosis ($P<0.05$), while no significant associations were observed for other genes (Fig. S2A). To further validate the prognostic independence of the model, both univariate and multivariate Cox regression analyses were performed for OS, DFI, PFI and DSS in the training cohort. The results demonstrated that LAGs were independent prognostic factors (all $P<0.05$; Figs. 4G and H; and S2B and C). Lastly, a nomogram integrating the risk score with key clinical parameters was constructed to quantitatively predict survival outcomes in patients with CESC (Fig. 4I). The nomogram analysis confirmed that the risk score significantly contributed to the highest prognostic weight ($P<0.001$), underscoring its clinical utility as a robust and independent predictor of cervical cancer prognosis.

Molecular mechanisms underlying LAGs-based subtype classification. To further elucidate the molecular mechanisms that associate LAGs with the prognosis of cervical cancer, functional annotation analyses were performed across the identified LAGs-derived molecular subtypes. In the low-risk group, Gene Set Variation Analysis (GSVA) revealed significant enrichment of biological pathways associated with 'receptor ligand activity, 'signaling receptor activator activity' and 'cell adhesion molecule binding' (Fig. 5A). KEGG pathway enrichment further demonstrated that the most enriched pathways were predominantly involved in energy metabolism, including 'central carbon metabolism in cancer', 'biosynthesis of amino acids' and 'glycolysis/gluconeogenesis' (Fig. 5B). Comparative GSVA between risk subgroups (Table SVI) indicated distinct molecular signatures: The high-risk group exhibited stronger activation of oncogenic and proliferative pathways, such as KRAS signaling downregulation, whereas the low-risk group displayed higher activity in immune- and stress-related pathways, including 'hypoxia', 'unfolded protein response' and 'angiogenesis' (Fig. 5C). Correlation analysis further confirmed that LAGs risk scores were significantly associated with these key signaling pathways (Fig. 5H). To assess the prognostic relevance of these pathways, Kaplan-Meier survival analyses were performed. Pathways negatively correlated with LAGs expression, such as cholesterol homeostasis, unfolded protein response, hypoxia and angiogenesis, were associated with favorable survival outcomes (Fig. 5D-G). By contrast, KRAS signaling downregulation, which was positively correlated with LAGs, was associated with poor prognosis (Fig. S2D). Collectively, these findings suggest that differential pathway activation between LAGs-defined subgroups reflects distinct metabolic and signaling landscapes, thereby elucidating potential molecular mechanisms by which LAGs contribute to cervical cancer progression.

Correlation between LAGs and single-cell characteristics. To investigate the role of LAG in the tumor immune microenvironment at the single-cell transcriptome level, the expression profiles of LAG prognostic genes were analyzed across distinct cell populations (Fig. 6A). Based on the LAGs prognostic model, tumor cells were categorized into high- and low-risk groups, followed by differential interaction analysis to examine intercellular communication patterns within the TME. Distinct cell-cell communication networks were observed between the two risk groups (Fig. 6B and C). Notably, intercellular signaling occurred among nearly all cell types (Fig. S2E), with particularly strong interactions detected between columnar and squamous epithelial cells. Functional annotation of ligand-receptor signaling revealed that the collagen, laminin and Notch pathways were predominantly enriched in highly cancerous cells, squamous and columnar epithelial cells, $CD4^+$ T cells and endothelial cells (Fig. 6D-F). These intercellular interactions are likely to regulate cell adhesion, migration and differentiation, thereby contributing to tumor progression and microenvironmental remodeling.

Since intratumoral heterogeneity is a major driver of tumorigenesis, progression, metastasis, therapeutic resistance and immune evasion, the present study next evaluated heterogeneity using the MATH score. Tumors with high LAGs risk exhibited markedly elevated MATH scores, indicating greater genomic instability (Fig. 6G). Furthermore, integrative analysis combining LAGs and MATH metrics revealed that patients in the high-risk and high-MATH score subgroup experienced significantly worse survival outcomes compared with those in the low-risk and low-MATH score subgroup (Fig. 6H; $P<0.001$). Collectively, these findings suggest that LAG activity is closely associated with alterations in cellular communication, tumor heterogeneity and the immune microenvironment, potentially influencing cervical cancer progression and patient prognosis.

Analysis of the tumor immune microenvironment in high- and low-risk LAGs groups. Immune infiltration serves a key role in tumor initiation, progression and therapeutic response, profoundly influencing the clinical outcomes of patients with cancer. To characterize the immune landscape

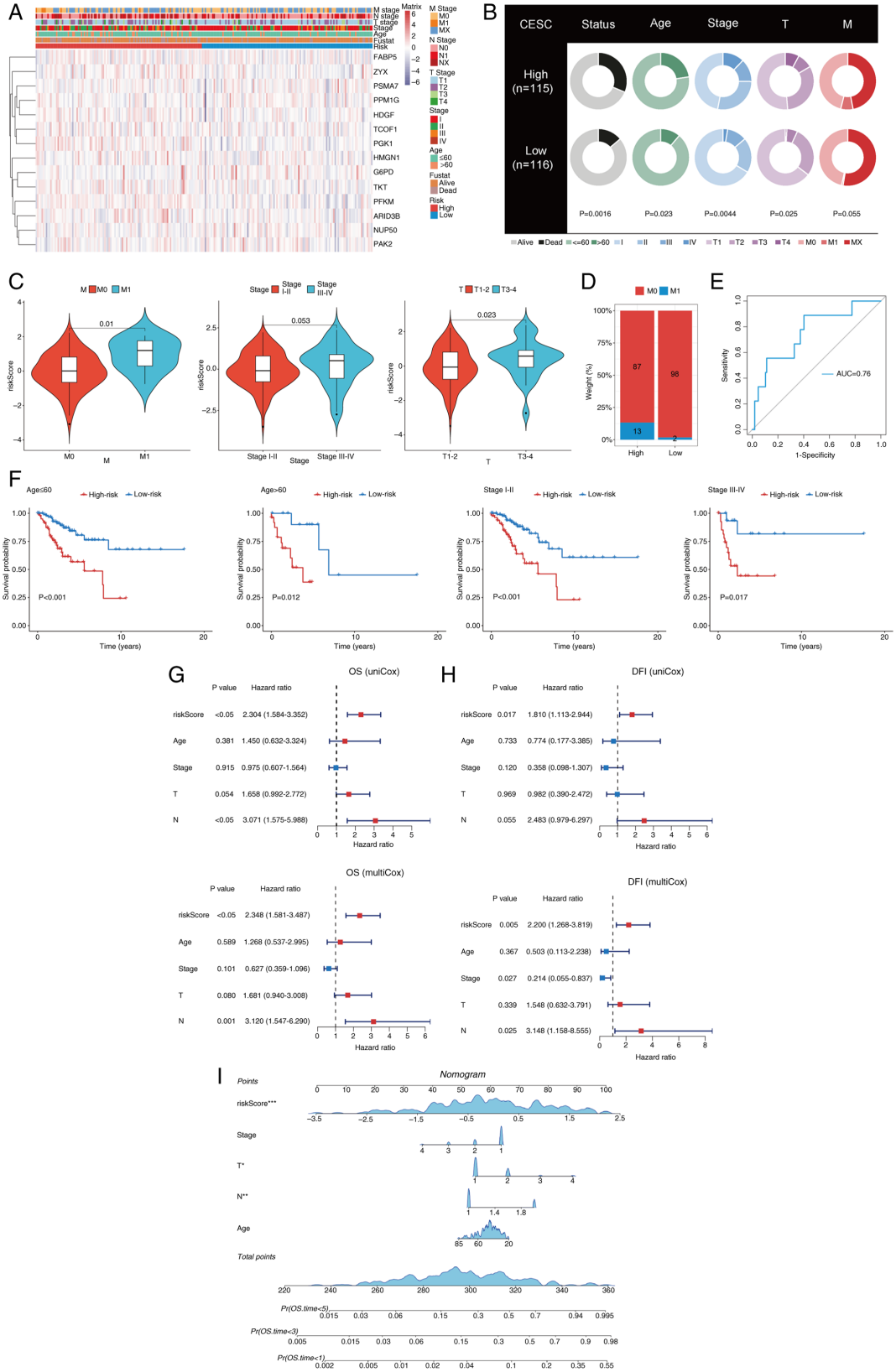

Figure 4. Predictive level of LAGs was analyzed based on clinical characteristics. (A) Distribution of clinical features based on LAGs risk scores and expression levels of model genes Purple indicates low expression, red indicates high expression. (B) Relationship between high- and low-LAGs risk groups and various clinical features. (C) Comparative analysis of risk scores across different M stage and T staging categories. (D) Distribution of M stage within LAGs risk groupings. (E) Receiver operating characteristic curves for the LAGs risk model in predicting M stage. (F) Kaplan-Meier survival curves demonstrating the consistent performance of LAGs across subgroups of patients with CESC, including age and stage. Univariate and multivariate Cox regression analyses of clinical characteristics of (G) OS and (H) DFI with LAGs in patients in The Cancer Genome Atlas-CESC cohort. (I) Column-line plots of the survival probabilities of patients at 1, 3 and 5 years were constructed in conjunction with the risk score of LAGs. *P<0.05, **P<0.01 and ***P<0.001. LAGs, lactylation-associated genes; CESC, cervical squamous cell carcinoma; OS, overall survival; DFI, disease-free interval; AUC, area under the curve; HMGN1, high-mobility group nucleosome-binding protein 1; TKT, transketolase; ZYX, zyxin; PAK2, p21 (RAC1) activated kinase 2; ARID3B, AT-rich interaction domain 3B; FABP5, fatty acid binding protein 5; HDGF, hepatoma-derived growth factor; T, tumor stage; N, lymph node stage.

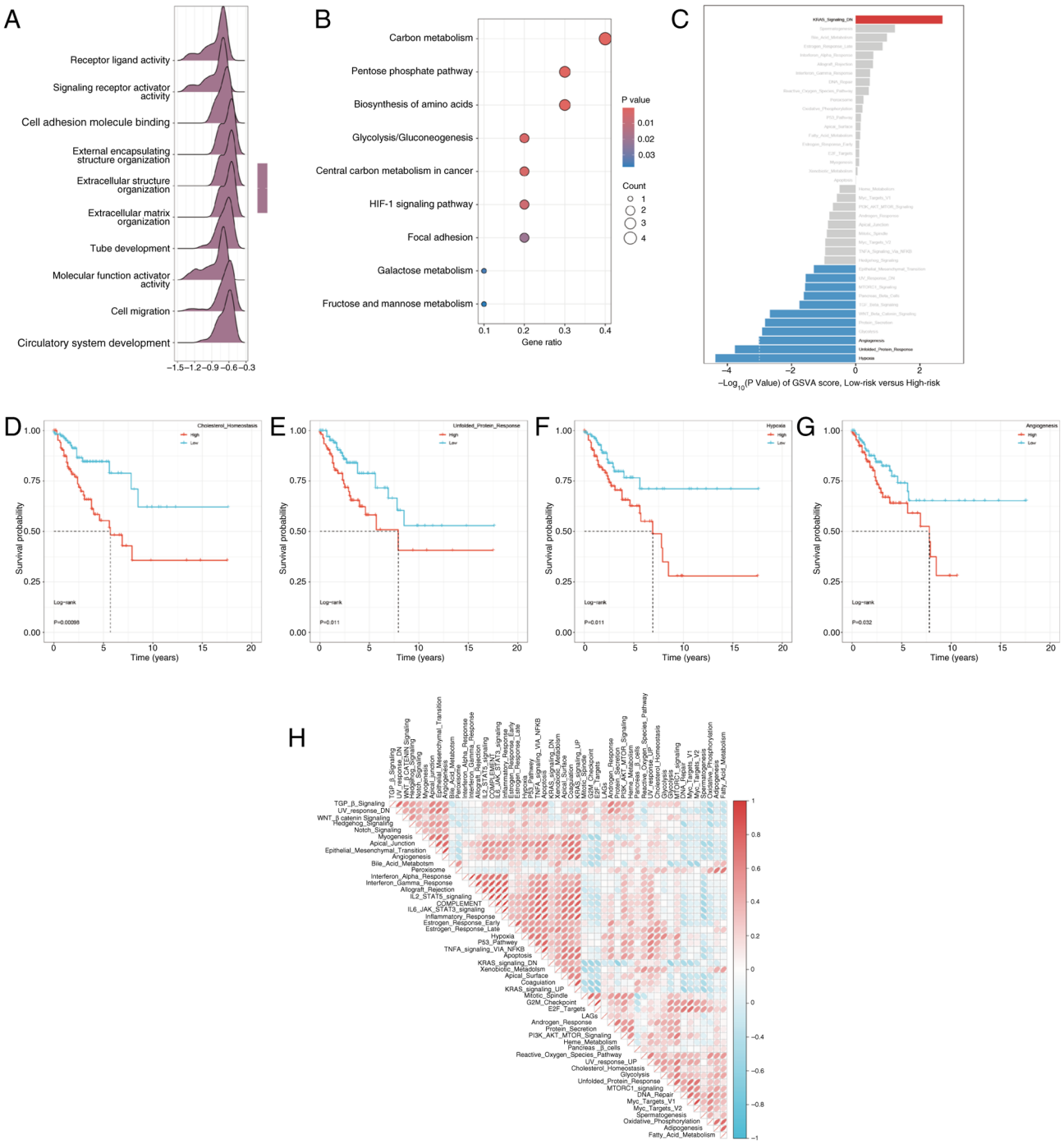

Figure 5. Functional enrichment analysis in different groupings of LAGs. (A) Mountain plot depicting Gene Ontology enriched pathways in the low-risk group. (B) Kyoto Encyclopedia of Genes and Genomes pathway analysis of risk subgroups for LAGs. (C) Differential analysis of marker signaling pathways between high-risk and low-risk groups based on GSVA scores. Kaplan-Meier survival analysis illustrates the prognostic impact of (D) cholesterol homeostasis, (E) unfolded protein response, (F) hypoxia and (G) angiogenesis signaling pathways. (H) Correlation analysis between LAGs risk scores and GSVA scores of characteristic signaling pathways. LAGs, ; GSVA, gene set variation analysis; HIF-1, hypoxia-inducible factor-1.

of cervical cancer, the present study calculated the immune, stromal and ESTIMATE scores for each sample (Fig. 7A). Although the high-risk group exhibited slightly elevated immune and stromal scores compared with the low-risk group, these differences did not reach statistical significance. Subsequently, ssGSEA was performed to evaluate immune pathway activities. The results demonstrated significant enrichment of the 'antigen processing and presentation' pathway and the 'NOD-like receptor signaling' pathway in the high-risk group (Fig. 7B). To further elucidate the immune cell composition, the abundance of tumor-infiltrating immune cells was quantified across samples. Activated B cells, eosinophils and immature B cells were predominantly enriched in the low-risk group, displaying significant intergroup differences (Fig. 7C). These findings were independently validated using the CIBERSORT algorithm, which yielded consistent results (Fig. 7D). Spearman correlation analysis identified nine immune cell

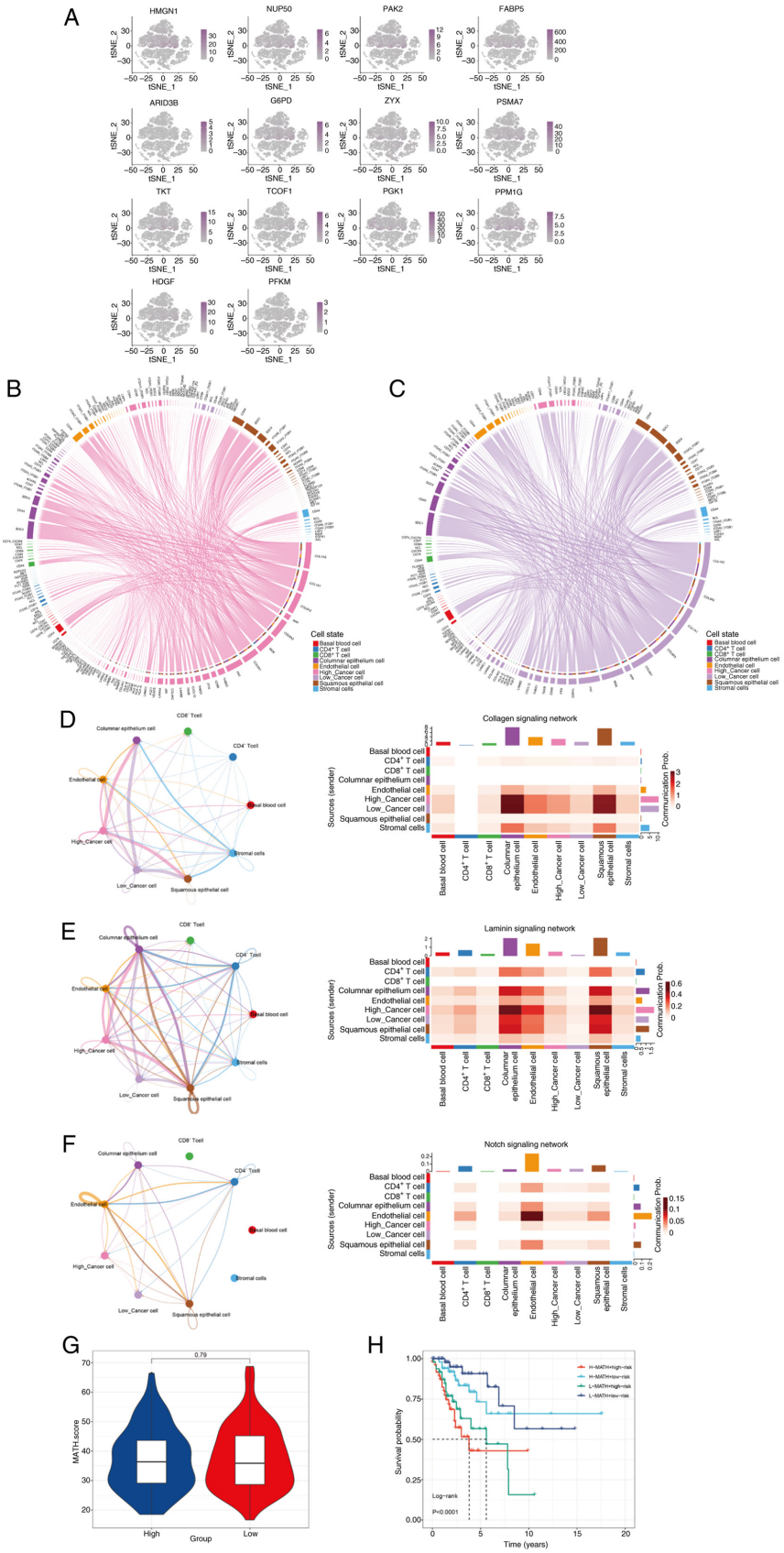

Figure 6. Correlation of the LAGs with single-cell characteristics. (A) Distribution of prognostic gene expression of LAGs in the single-cell transcriptome. The shade of color indicates the distribution level of LAGs within cells, ranging from light purple (low expression) to dark purple (high expression). (B) Cellular communication network diagram for high-risk tumor cells. (C) Cellular communication network diagram for low-risk tumor cells. Network diagrams of the (D) collagen, (E) laminin and (F) notch signaling pathways, where the circle plots illustrate the communication network and the heatmaps indicate the proportion of different cell types within the network. (G) Comparison of MATH tumor heterogeneity scores between high-risk and low-risk groups. (H) Overall survival analysis using MATH scores combined with LAGs. LAGs, lactylation-associated genes; HMGN1, high-mobility group nucleosome-binding protein 1; TKT, transketolase; ZYX, zyxin; MATH, mutant-allele tumor heterogeneity; PAK2, p21 (RAC1) activated kinase 2; ARID3B, AT-rich interaction domain 3B; FABP5, fatty acid binding protein 5; HDGF, hepatoma-derived growth factor.

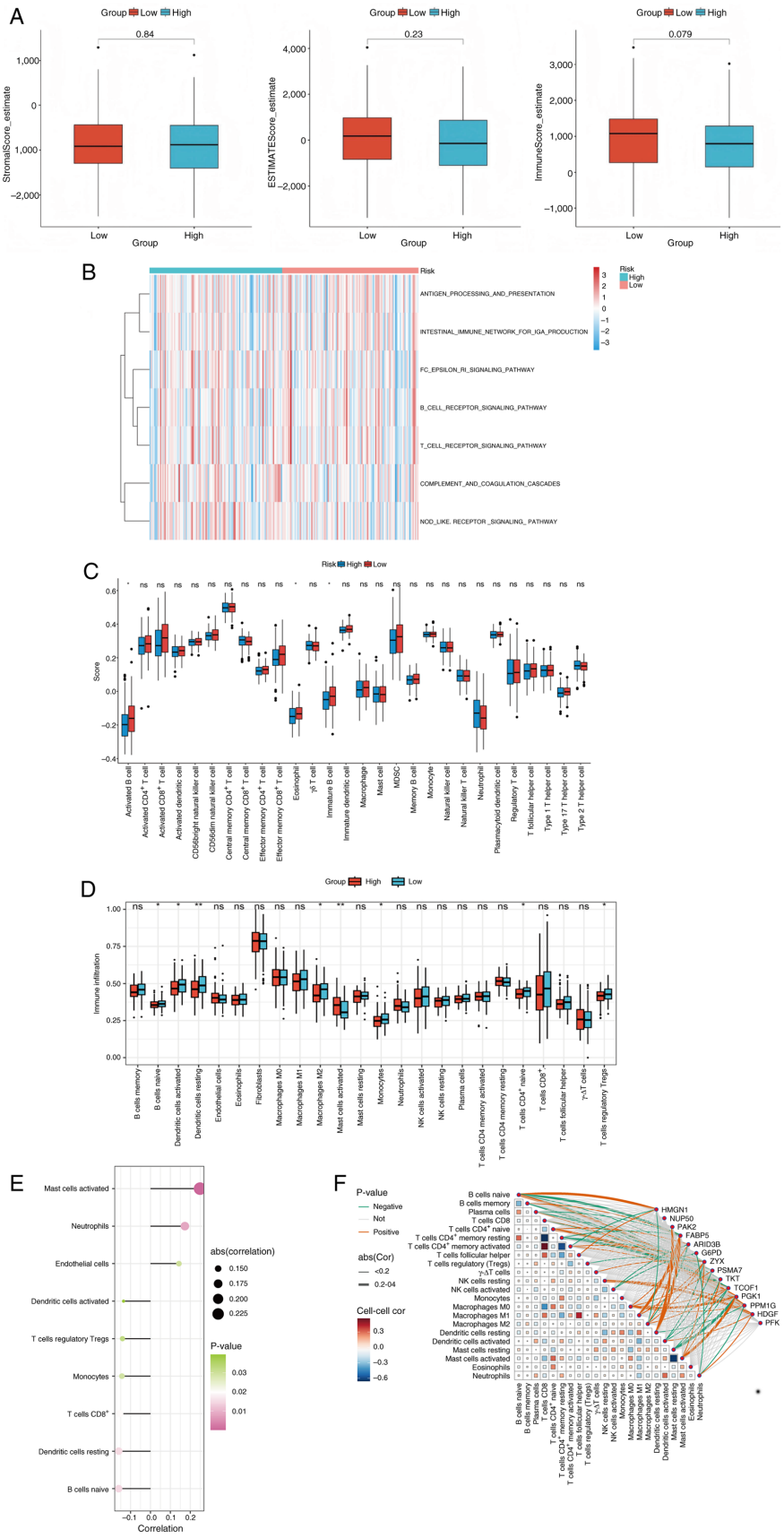

Figure 7. Correlation of prognostic risk models for LAGs with the immune environment. (A) Comparison of immune status between high-risk and low-risk groups based on immune, stromal and ESTIMATE scores. (B) Heatmap depicting the differences in activity scores of immune-related pathways between high-risk and low-risk groups. (C) Assessment of immune cell infiltration abundance in high-risk and low-risk groups using the single sample Gene Set Enrichment Analysis algorithm. (D) Quantification of differences in immune cell abundance between high-risk and low-risk groups using the Cell-type Identification by Estimating Relative Subsets of RNA Transcripts algorithm. (E) Correlation analysis between immune cell infiltration and risk scores. (F) Correlation analysis between immune cell types and the prognostic genes of LAGs. *P<0.05 and **P<0.01. ns, not significant; LAGs, lactylation-associated genes; NK, natural killer; HMGN1, high-mobility group nucleosome-binding protein 1; TKT, transketolase; ZYX, zyxin.

subtypes significantly associated with LAGs risk scores (Fig. 7E). Furthermore, correlation analyses between LAGs prognostic genes and specific immune cell populations revealed that AT-rich interaction domain 3B, phosphoglycerate kinase 1 (PGK1) and protein phosphatase, Mg^{2+}/Mn^{2+} dependent 1G (PPM1G) were positively correlated with M0 macrophages and activated mast cells and indicated widespread associations with monocyte-related gene expression (Figs. 7F and S2F). Lastly, the relationship between TME infiltration and OS was examined and six immune cell subtypes were significantly associated with patient prognosis (log-rank test; P<0.05; Fig. S2G-L), including M0 and M1 macrophages, resting mast cells, CD8, γΔ and regulatory T cells. Collectively, these findings indicate that the LAGs risk signature is closely associated with alterations in the immune landscape of cervical cancer, potentially influencing both tumor immunity and clinical outcomes.

Association between LAGs risk subgroups, drug sensitivity and immunotherapy response. To further assess the clinical utility of the LAGs-based risk model in guiding treatment strategies, the present study explored its association with immunotherapy response and drug sensitivity. Using the IMvigor210 cohort, the present study evaluated the predictive value of the LAGs risk score for immunotherapy efficacy. The distribution of clinical responses-including complete remission (CR), partial remission (PR), stable disease (SD) and progressive disease (PD)-was compared between risk subgroups using χ^2 tests. The high-risk group exhibited a markedly higher proportion of PD/SD cases, whereas CR/PR responses were significantly more frequent in the low-risk group (Fig. 8A). Consistently, patients achieving CR/PR demonstrated significantly lower risk scores compared with those with SD/PD, suggesting that lower LAGs scores are associated with more favorable immunotherapeutic outcomes (Fig. 8B and C). To evaluate chemotherapeutic drug sensitivity, the IC_{50} values of various agents were compared between high- and low-risk subgroups. The risk score exhibited a significant positive correlation with the IC_{50} values of paclitaxel (R=0.16; P<0.05) and rapamycin (R=0.26; P<0.05) (Fig. 8D and E) and a negative correlation with midostaurin (Fig. 8F; R=-0.32; P<0.05). Specifically, paclitaxel and rapamycin displayed lower IC_{50} values in the low-risk group, indicating higher predicted sensitivity, while midostaurin demonstrated higher IC_{50} values in the high-risk group, suggesting potential efficacy in these patients (Fig. 8G-I).

Furthermore, to validate the expression of LAGs *in vitro*, the present study measured mRNA expression levels of the 14 LAGs included in the prognostic model using RT-qPCR in HaCaT epithelial cells and cervical squamous carcinoma cell lines (SiHa and HeLa). The results revealed that the majority of genes, including G6PD, HMGN1, ZYX, PAK2, TCOF1 and TKT, were significantly upregulated in cervical cancer cells compared with normal epithelial cells (Fig. 8J). Therefore, these findings demonstrate that the LAGs-based prognostic model not only stratifies patients by survival risk but also provides notable insights into immunotherapy responsiveness and chemotherapeutic sensitivity, thereby offering a potential framework for personalized treatment optimization in cervical cancer in the future.

MR analysis demonstrates a causal relationship between the LAGs prognostic model and cervical cancer. To further investigate the relationship between the LAG prognostic model and cervical cancer and to determine whether this relationship is causal or merely correlative, the present study performed a two-sample MR analysis. In this analysis, prognostic genes were used as exposure factors and cervical cancer was the outcome. The present study was unable to obtain identifiers for several genes, including glucose-6-phosphate dehydrogenase, proteasome subunit α type 7, treacle ribosome biogenesis factor 1, PGK1, PPM1G and PFKM, as certain genes lacked sufficient SNPs, leading to their exclusion from the analysis. Using the IVW method (Table I), the present study identified HMGN1 as a protective factor, with an odds ratio of 0.81 (95% CI, 0.70-0.94; P=0.0051; Fig. 9A and D). However, no significant causal relationship was observed between zyxin (ZYX) and TKT (P>0.05; Fig. 9B and C, E and F).

To assess the robustness of the present analysis, funnel plots were constructed using the β coefficients and SEs for each IV associated with the three genes studied (Fig. 9G-I). The distributions of these plots revealed certain asymmetry, possibly due to the limited number of IVs, which may introduce heterogeneity and potential bias. To account for this, the present study performed heterogeneity tests, all of which yielded P>0.05, indicating that heterogeneity did not significantly affect the present study results (Table SVII). Furthermore, the present study conducted leave-one-out analyses to assess the stability of the present study findings. The results remained consistent even after excluding individual SNPs, further supporting the robustness of the associations (Fig. 9J-L). The present study also performed a test for horizontal pleiotropy on HMGN1, with P>0.05, indicating no significant evidence of horizontal pleiotropy influencing the present study results (Table SVIII). The present study results provide strong evidence for a causal relationship between HMGN1 and cervical cancer, while no significant MR associations were observed for the other analyzed genes. These findings highlight the potential role of HMGN1 in the pathogenesis of cervical cancer.

HMGN1 can serve as a therapeutic target for patients with CESC. To further investigate the role of HMGN1 in cervical cancer, the present study designed HMGN1-specific siRNA sequences using siRNA technology and transfected them into SiHa and HeLa cells. Subsequently, 24 h after transfection, the present study assessed the knockdown efficiency of HMGN1 using RT-qPCR, which confirmed that HMGN1 was successfully silenced in both cell lines (Fig. 10A). Subsequent western blotting was performed to assess the protein expression of HMGN1, further validating the effectiveness of the knockdown (Fig. 10B). Functional assays revealed that inhibition of HMGN1 significantly suppressed the proliferation of SiHa and HeLa cells (Fig. 10C), reduced the proportion of S-phase cells and prolonged the G_2 phase of the cell cycle (Fig. 10D). Therefore, these findings suggest that HMGN1 may be a risk factor for CESC.

Discussion

Cervical cancer is a prevalent and aggressive malignancy in women, marked by high recurrence and metastasis rates that lead

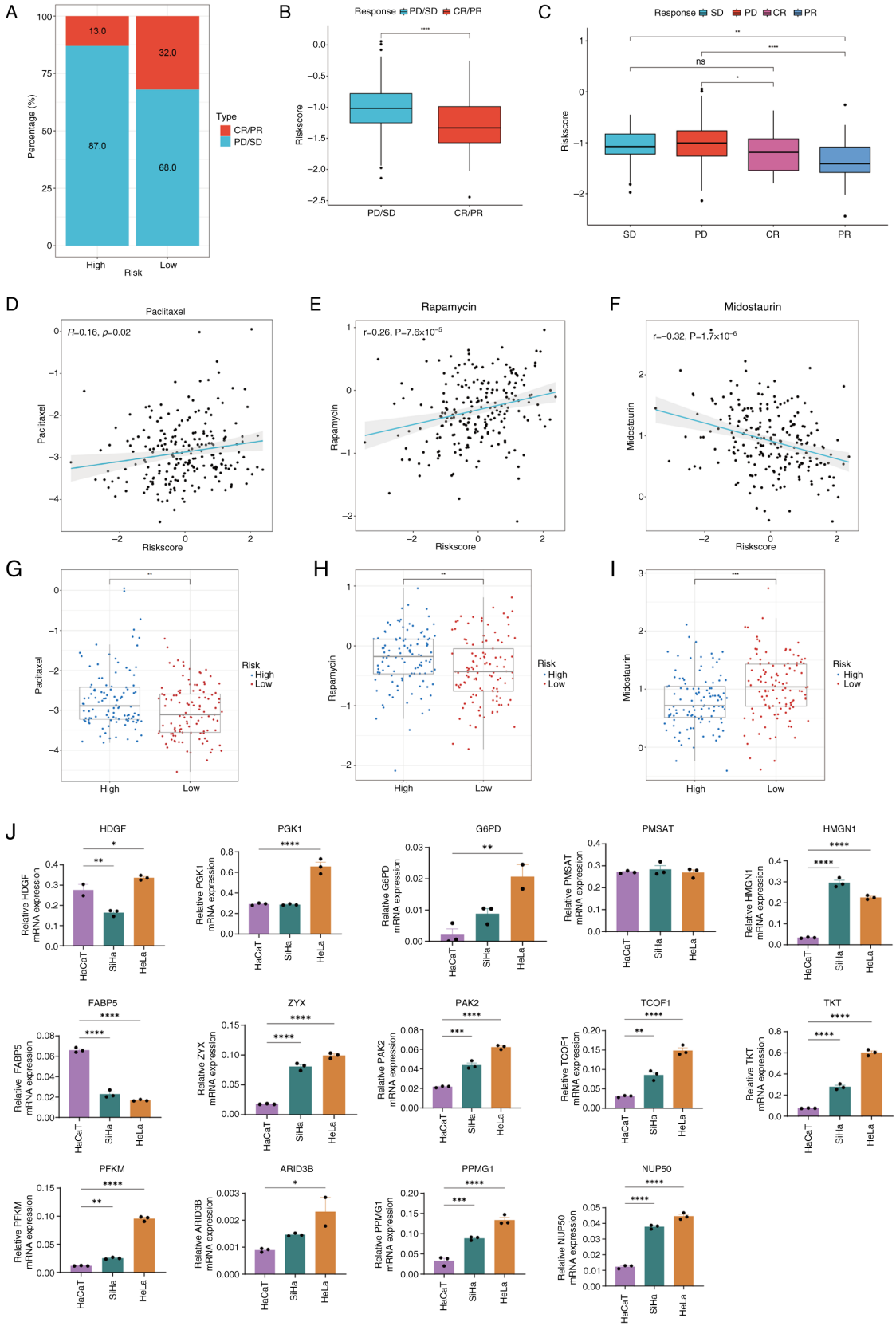

Figure 8. Analysis of LAGs risk subgroups in relation to drug sensitivity and immunotherapy response. (A) Proportion of patients with CR/PR or SD/PD receiving immunotherapy in the high- and low-risk groups of the IMvigor210 cohort. (B) Box plot illustrating the difference in risk scores between patients with CR/PR and those with SD/PD in the IMvigor210 cohort. (C) Box plot depicting the distribution of risk scores among CR, PR, SD and PD patients in the IMvigor210 cohort. Correlation between LAGs-related risk scores and half-maximal inhibitory concentrations of (D) paclitaxel, (E) rapamycin and (F) midostaurin. Comparison of drug sensitivity between high- and low-risk groups for (G) paclitaxel, (H) rapamycin and (I) midostaurin. (J) mRNA expression levels of genes associated with the LAGs prediction model. *P<0.05, **P<0.01, ***P<0.001 and ****P<0.0001. ns, not significant; LAGs, lactylation-associated genes; CR, complete remission; PR, partial remission; SD, stable disease; PD, progressive disease; HMGN1, high-mobility group nucleosome-binding protein 1; TKT, transketolase; ZYX, zyxin; PAK2, p21 (RAC1) activated kinase 2; ARID3B, AT-rich interaction domain 3B; FABP5, fatty acid binding protein 5; HDGF, hepatoma-derived growth factor.

Table I. MR analysis of the LAGs prognostic model from the finngen_R12_CD2_INSITU_CERVIX_UTERI_EXALLC data source.

Exposure	Gene	Method	Number of SNPs	β	SE	P-value	OR	or_lci95	or_uci95
Carcinoma *in situ* of cervix uteri	HMGN1	Inverse variance weighted	20	-0.208311264	0.074517941	0.005182733	0.811954265	0.701617827	0.939642214
		MR Egger		-0.935886258	0.451742896	0.174083585	0.392238087	0.161814877	0.950782279
		Simple mode		-0.090818216	0.157267515	0.604106442	0.913183698	0.670948735	1.242873595
		Weighted mode		-0.264655633	0.086377683	0.054823054	0.767470196	0.647940834	0.909049825
		Weighted median		-0.216692908	0.077847357	0.005376567	0.805177195	0.691236174	0.937899867
	NUP50	Inverse variance weighted	2	-0.004228927	0.094542495	0.964322174	0.995780002	0.827346061	1.198504301
	TKT	Inverse variance weighted	20	-0.000368019	0.0557443	0.994732468	0.999632048	0.89616848	1.115040592
		MR Egger		0.107180793	0.08810701	0.347880425	1.113135483	0.936590667	1.322958522
		Simple mode		0.038402893	0.11447086	0.759352482	1.039149815	0.830306813	1.300522073
		Weighted mode		0.031367274	0.05042089	0.577947782	1.031864411	0.934767287	1.139047309
		Weighted median		0.021688186	0.047296271	0.646550039	1.021925085	0.931450245	1.121188044
	ZYX	Inverse variance weighted	20	-0.049281896	0.06806318	0.469028271	0.951912752	0.833029912	1.087761524
		MR Egger		-0.103085931	0.160727915	0.586973835	0.902049456	0.658288072	1.236074684
		Simple mode		-0.045157699	0.118377715	0.728268287	0.955846734	0.75791956	1.205461669
		Weighted mode		-0.022977045	0.091040541	0.817049205	0.977284917	0.817571837	1.16819803
		Weighted median		-0.024763227	0.07300978	0.73447651	0.975540867	0.845470167	1.125622191
	PAK2	Inverse variance weighted	2	0.10067654	0.252150728	0.689693339	1.105918863	0.674665081	1.812835086
	ARID3B	Wald ratio	1	0.047089984	0.132516165	0.722325339	1.048216328	0.808445752	1.359098576
	FABP5	Wald ratio	1	0.072237589	0.073148103	0.32337188	1.0749107	0.931338302	1.240615801
	HDGF	Wald ratio	1	0.425897326	0.181286783	0.018808666	1.530963576	1.073125298	2.18413402

MR, Mendelian randomization; LAGs, lactylation-related genes; OR, odds ratio; HMGN1, high-mobility group nucleosome-binding protein 1; NUP50, nucleoporin 50; TKT, transketolase; ZYX, zyxin; PAK2, p21 (RAC1) activated kinase 2; ARID3B, AT-rich interaction domain 3B; FABP5, fatty acid binding protein 5; HDGF, hepatoma-derived growth factor; SNPs, single nucleotide polymorphisms.

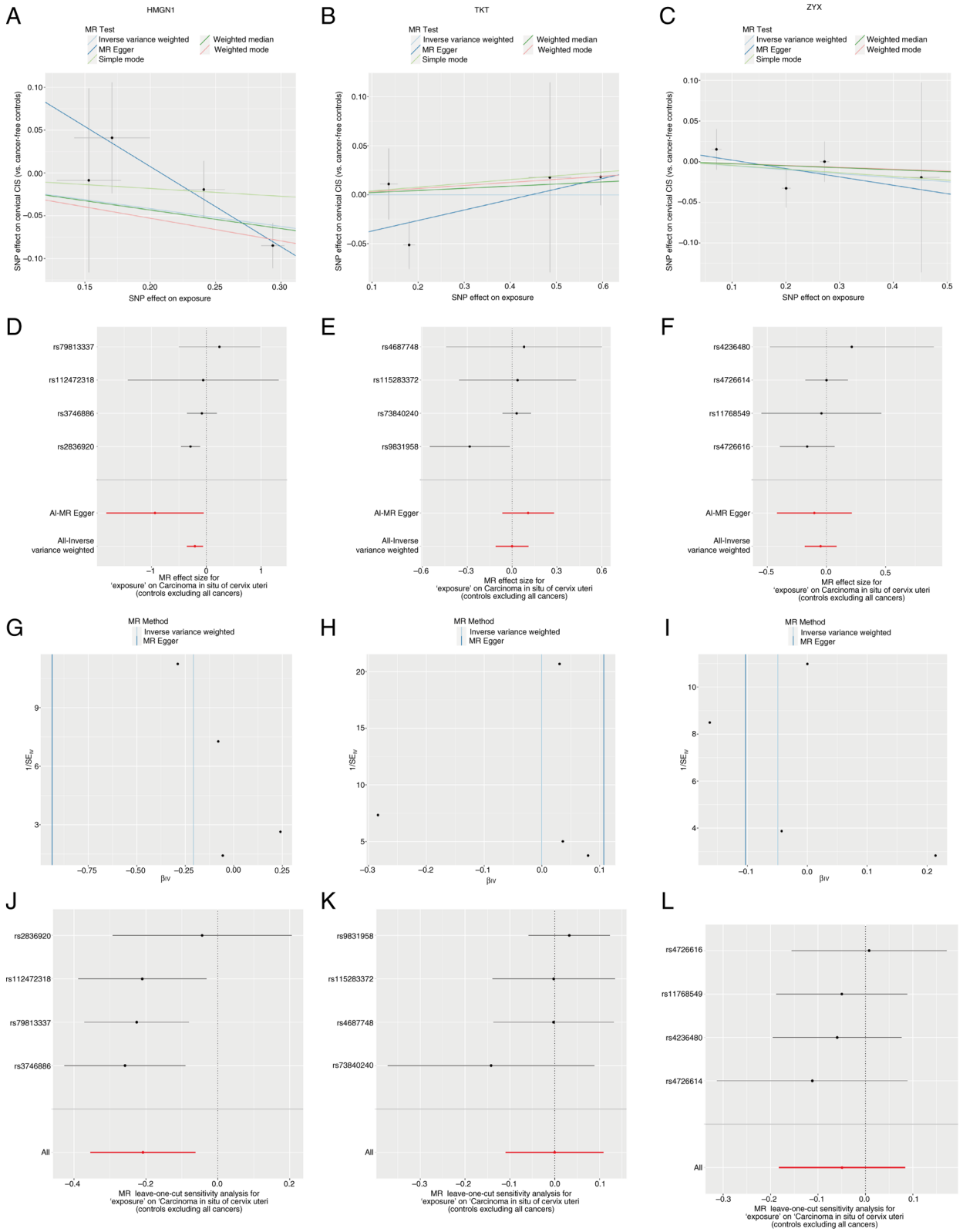

Figure 9. MR analysis demonstrates a causal relationship between the LAGs prognostic model and cervical cancer. MR scatter plots display the association between (A) HMGN1, (B) TKT, (C) ZYX and patients with cervical cancer. Forest plots depicting the overall effect of (D) HMGN1, (E) TKT and (F) ZYX on cervical cancer. Funnel plots for (G) HMGN1, (H) TKT and (I) ZYX in cervical cancer. Leave-one-out analysis of the remaining stability after excluding (J) HMGN1, (K) TKT and (L) ZYX SNPs. SNPs, single nucleotide polymorphisms; HMGN1, high-mobility group nucleosome-binding protein 1; TKT, transketolase; ZYX, zyxin; MR, Mendelian randomization.

to poor outcomes (52). Although TNM staging and histopathological grading are extensively used, their prognostic accuracy and value for individualized therapy remain limited (53,54). Therefore, identifying novel prognostic biomarkers is key to improve risk stratification and advance precision medicine in cervical cancer management in the future.

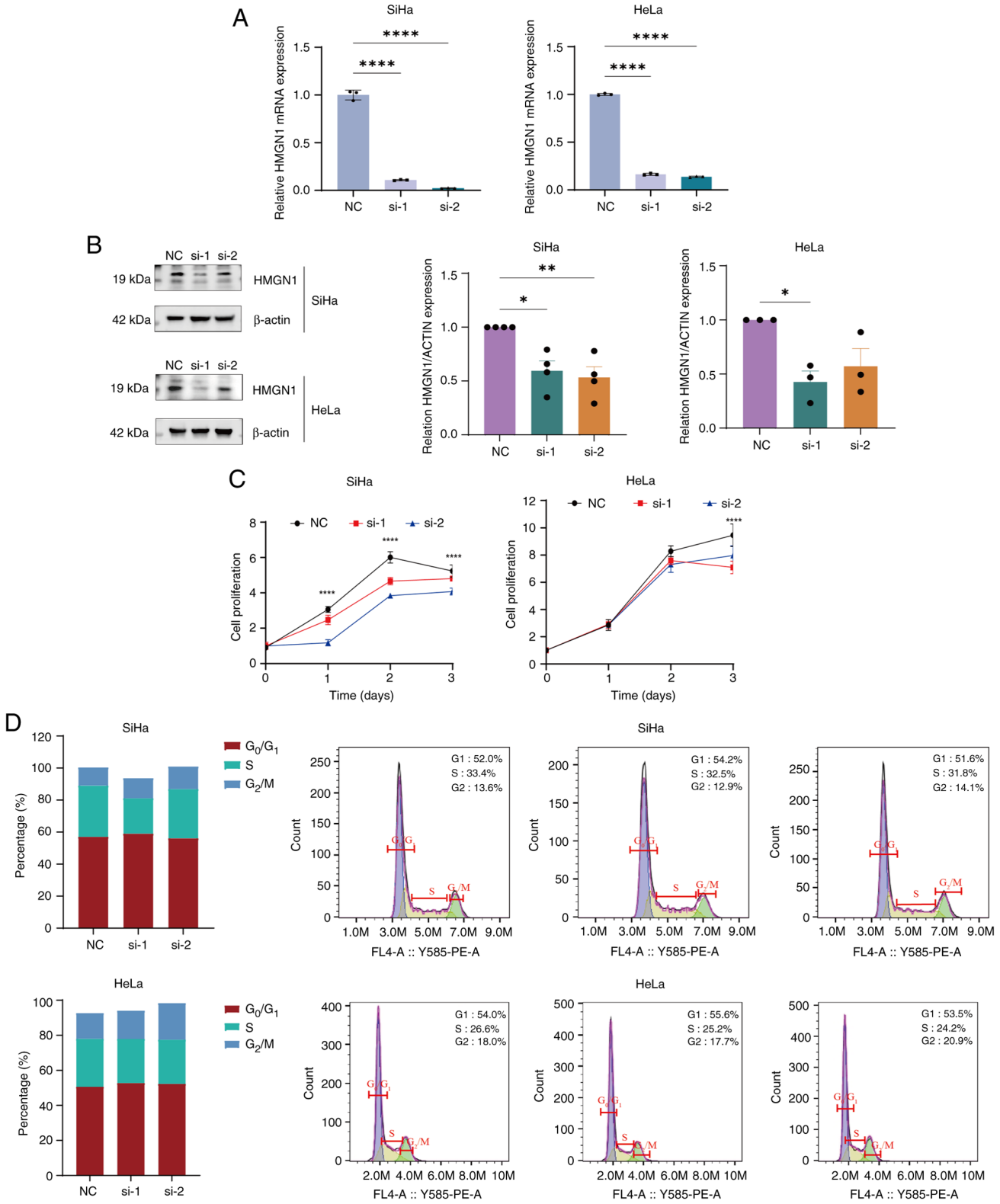

Figure 10. HMGN1 inhibition affects the proliferation of cervical squamous cells. (A) mRNA and (B) protein expression levels of HMGN1 in SiHa and HeLa cells following siRNA transfection, compared with the NC. (C) Cell Counting Kit-8 assay assessing the proliferation of SiHa and HeLa cells at 24, 48 and 72 h. (D) Cell cycle distribution of SiHa and HeLa cells after HMGN1 inhibition was analyzed by flow cytometry, including flow cytometry plots and quantitative histograms. *P<0.05, **P<0.01 and ****P<0.001. HMGN1, high-mobility group nucleosome-binding protein 1; NC, non-targeting control; si, small interfering RNA.

Lactylation, an epigenetic post-translational modification on lysine residues, regulates protein function and participates in key cellular processes such as metabolism, immune regulation and signal transduction (24-26). Increasing evidence associate abnormal lactylation with tumorigenesis and cancer progression (55-57). In the present study, TCGA-CESC and GEO

datasets were integrated to identify 43 LAGs associated with cervical cancer prognosis and a 14-gene prognostic model was developed using multiple machine learning algorithms (CoxBoost, StepCox, RSF and LASSO). The model demonstrated independent predictive performance for OS, DFI, PFI and DSS, surpassing conventional clinical factors such as age, stage and T classification. To ensure generalizability and reduce overfitting, it was externally validated in the GSE30760 cohort and key genes were further confirmed in GSE7803 using AUC analysis. Consistent performance across datasets demonstrated its robustness and clinical utility. This risk scoring system provides a potential practical framework for patient stratification-high-risk patients may require intensive therapy or closer follow-up, whereas low-risk patients could benefit from less aggressive management.

Functional enrichment analysis elucidated the biological mechanisms underlying the prognostic relevance of LAGs in cervical cancer. GSVA analysis revealed that the low-risk group was enriched in pathways associated with 'TNFA signaling via NF-KB', 'hypoxia', 'unfolded protein response' and 'angiogenesis', while the high-risk group exhibited activation of the KRAS signaling pathway. These pathways are key mediators of tumor cell proliferation, invasion and immune regulation (27-29). Previous studies have indicated that human papilloma virus (HPV) type 16 E2 protein enhances TNF-α-induced NF-κB activation, promoting cervical tumor progression; whereas hypoxia-inducible factor-1α and VEGF drive hypoxia-induced angiogenesis and metastasis (58,59). Similarly, mutations in the MAPK/ERK cascade (common in gynecological cancer) also support the involvement of these oncogenic pathways (60). KEGG and GO analyses further revealed enrichment in 'carbon metabolism', 'glycolysis/gluconeogenesis' and 'amino acid biosynthesis', highlighting the role of metabolic reprogramming in LAG-mediated tumor progression. Consistent with a previous study by Tong *et al* (8), the present study findings indicated that lactylated histones both promote glycolytic metabolism and regulate immune homeostasis, suggesting LAGs may cascade metabolic activation with immune evasion in cervical cancer. Notably, aerobic glycolysis enhances tumor metastasis and chemotherapy resistance (61). The myosin regulatory light polypeptide 9 protein promotes glycolysis (62), while celecoxib combined with cisplatin or paclitaxel inhibits tumor growth by disrupting energy metabolism (63). Collectively, these findings suggest that LAGs may drive cervical cancer progression by coordinating metabolic and immune regulatory pathways, providing a theoretical basis for metabolic and immune-targeting therapeutic strategies.

Single-cell transcriptomic analysis further revealed the expression of LAGs in various cell types, including columnar and squamous epithelial cells, $CD4^+$ T cells and tumor cells, highlighting their involvement in cervical cancer progression and the immune response. Cell-cell communication analysis further identified significant associations between Notch, laminin and collagen signaling pathways and LAGs-based risk subgroups. These pathways modulate ECM interactions, influence tumor cell adhesion and migration, and impede immune cell communication, thereby promoting tumor progression (64). Among them, Notch signaling is a key driver of tumorigenesis and is associated with poor prognosis in cervical cancer (65). Laminin enhances migration and differentiation through PI3K/AKT and MAPK pathways, which are dysregulated by HPV oncoproteins (E5, E6 and E7) (66). Similarly, aberrant MAPK activation promotes proliferation and survival through the AKT/mTOR/pyruvate dehydrogenase kinase 1 axis (67). Collectively, these findings underscore that integrating single-cell transcriptomic data with molecular profiling provides key insights into the microenvironmental mechanisms underlying cervical cancer and informs potential therapeutic strategies.

Immunotherapy has emerged as a promising therapeutic strategy for cervical cancer by reshaping the tumor immune microenvironment and addressing tumor heterogeneity, thereby enabling early molecular stratification and personalized intervention (52). In the present study, immune infiltration analysis revealed that the low-risk group exhibited higher levels of activated immune cells, including B and mast cells, M2 macrophages and monocytes, compared with the high-risk group, indicating a more active antitumor immune response. By contrast, the high-risk group displayed an immunosuppressive microenvironment, which may contribute to worse clinical outcomes. These findings are consistent with previous studies that reported M2 macrophage infiltration is associated with immune escape and unfavorable prognosis in cervical cancer (68,69). Furthermore, analysis of the IMvigor210 real-world immunotherapy cohort supported these observations: Low-risk patients achieved higher rates of CR/PR, while high-risk patients were more likely to experience disease SD/PDs. Drug sensitivity analysis further revealed that paclitaxel and rapamycin exhibited greater predicted efficacy in the low-risk group, whereas midostaurin was more effective in the high-risk group. Mechanistically, the paclitaxel-platinum combination remains the standard first-line regimen for cervical cancer and rapamycin-an mTOR pathway inhibitor-may suppress tumor growth through metabolic reprogramming (70).

Notably, the LAGs-based model also provides mechanistic insight into how immune cell composition influences therapeutic response. In the high-risk group, the TME is dominated by immunosuppressive M2 macrophages that inhibit $CD8^+$ T cell activation, thereby reducing cytotoxicity and promoting resistance to immune checkpoint inhibitors. These findings suggest that high-risk patients might benefit more from combination regimens that both block immune checkpoints (for example, programmed cell death protein-1/programmed cell death-ligand 1 inhibitors) and modulate macrophage polarization to restore an inflammatory (M1-like) phenotype. By contrast, the low-risk group demonstrated higher infiltration of activated $CD8^+$ T cells, which are key to antitumor cytotoxicity. Such patients may be more responsive to ICI monotherapy or therapeutic strategies aimed at further enhancing $CD8^+$ T cell activity. Collectively, these findings demonstrate that the LAGs-based prognostic model not only stratifies patients by survival risk but also provides key guidance for immunotherapy selection and chemotherapy optimization. By integrating immune and metabolic profiling, the present study model supports the development of personalized treatment strategies and precision medicine frameworks for CESC.

Using MR analysis, the present study investigated the causal relationship between lactose-associated genes (LAGs) and cervical cancer. Using IVW, weighted median and MR-Egger regression analyses, the present study identified a significant causal association between HMGN1 expression and cervical cancer risk. Other prognostic genes demonstrated no causal effects, potentially due to genetic or environmental influences. Previous studies confirm the key role of HMGN1 in DNA repair, genomic stability and tumor immune microenvironment regulation (39-42). *In vitro* experiments further validated that silencing HMGN1 in SiHa and HeLa cells inhibits cell proliferation and S-phase progression, highlighting its potential as a therapeutic and prognostic target for cervical cancer. Several limitations warrant attention: *In vitro* validation was limited to HPV-positive cell lines and primarily focuses on proliferation studies, without addressing other carcinogenic processes such as cell migration and invasion. Future research should extend to HPV-negative models and patient-derived models to conduct more detailed investigations. Larger multi-ethnic GWAS and comprehensive eQTL datasets will enhance causal inference. The proposed prognostic model stratifies patients into high-risk and low-risk groups to guide treatment intensity-high-risk patients may require more aggressive therapy or closer monitoring, while low-risk patients can receive lower-intensity management. External validation in independent cohorts and optimization of risk thresholds are essential prior to clinical implementation. Integration into hospital information systems could enable automated risk prediction, while prospective clinical trials are needed to confirm its impact on survival rates and quality of life. Collaboration with diagnostic reagent developers to establish standardized LAG testing protocols will further advance clinical translation and promote precision management of cervical cancer.

The present study established a 14-gene prognostic model based on LAGs using an integrative multi-omics analysis of cervical cancer. The model accurately predicts patient outcomes and exhibits strong associations with immune cell infiltration, tumor heterogeneity, cell-cell communication and drug sensitivity. Furthermore, HMGN1 was identified as a key gene with a causal role in cervical cancer and potential as a therapeutic target, emphasizing its importance in tumor progression. Collectively, these findings provide novel insights into the molecular mechanisms underlying cervical cancer and highlight the clinical utility of LAGs for both prognostic assessment and personalized treatment strategies in the future.

Acknowledgements

Not applicable.

Funding

The present study was funded by The National Natural Science Foundation of China (grant no. 82074478), Key program of Administration of Traditional Chinese Medicine of Jiangsu Province, China (grant no. ZX202102), Jiangsu Province Leading Talents Cultivation Project for Traditional Chinese Medicine (grant no. SLJ0307).

Availability of data and materials

The data generated in the present study may be requested from the corresponding author.

Authors' contributions

RW contributed to writing, conceptual design and methodology development. LN was involved in writing, draft preparation, bioinformatics analysis, and experimental research. XL contributed to writing, software application and data collection. YX and YS participated in methodology development and visualization. QR and HZ contributed to conceptual design, writing, review, and editing. RW also contributed to software application and data acquisition. RW and LN participated in data validation and analysis. QR contributed to study design and supervision. LN and RW confirm the authenticity of the raw data. All authors read and approved the final version of the manuscript.

Ethics approval and consent to participate

Not applicable.

Patient consent for publication

Not applicable.

Competing interests

The authors declare that they have no competing interests.

References

1. Bray F, Laversanne M, Sung H, Ferlay J, Siegel RL, Soerjomataram I and Jemal A: Global cancer statistics 2022: GLOBOCAN estimates of incidence and mortality worldwide for 36 cancers in 185 countries. CA Cancer J Clin 74: 229-263, 2024.
2. Wisniak A, Yakam V, Bolo SE, Yakam V, Schmidt NC, Kenfack B and Petignat P: Fertility and miscarriage incidence after cervical intraepithelial neoplasia treatment by thermal ablation: A cohort study. BMC Womens Health 132: 167-177, 2025.
3. Duenas-Gonzalez A, Serrano-Olvera A, Cetina L and Coronel J: New molecular targets against cervical cancer. Int J Women Health 6: 1023-1031, 2014.
4. Wei F, Georges D, Man I, Baussano I and Clifford GM: Causal attribution of human papillomavirus genotypes to invasive cervical cancer worldwide: A systematic analysis of the global literature. Lancet 404: 435-444, 2024.
5. Malagón T, Franco EL, Tejada R and Vaccarella S: Epidemiology of HPV-associated cancers past, present and future: Towards prevention and elimination. Nat Rev, Clin Oncol 21: 522-538, 2024.
6. Caruso G, Wagar MK, Hsu HC, Hoegl J, Rey Valzacchi GM, Fernandes A, Cucinella G, Sahin Aker S, Jayraj AS, Mauro J, *et al*: Cervical cancer: A new era. Int J Gynecol Cancer 34: 1946-1970, 2024.
7. Zhang Y, Lu Y, Li S, Zheng F, Dong Y, Tang H, Wang X and Wang J: Precision theranostics in cervical Cancer: Harnessing stimuli-responsive hydrogels for tumor microenvironment-targeted therapy and diagnosis. Materials Today Bio 35: 102392, 2025.
8. Tong H, Jiang Z, Song L, Tan K, Yin X, He C, Huang J, Li X, Ling X, et al: Dual impacts of serine/glycine-free diet in enhancing antitumor immunity and promoting evasion via PD-L1 lactylation. Cell Metab 36: 2493-2510, 2024.
9. Sia TY, Wan V, Finlan M, Zhou QC, Iasonos A, Zivanovic O, Sonoda Y, Chi DS, Long Roche K, Jewell E, *et al*: Procedural interventions for oligoprogression during treatment with immune checkpoint blockade in gynecologic malignancies: A case series. Int J Gynecol Cancer 34: 594-601, 2024.

10. Pinheiro C, Garcia EA, Morais-Santos F, Moreira MA, Almeida FM, Jubé LF, Queiroz GS, Paula ÉC, Andreoli MA, Villa LL, *et al*: Reprogramming energy metabolism and inducing angiogenesis: Co-expression of monocarboxylate transporters with VEGF family members in cervical adenocarcinomas. BMC Cancer 15: 835, 2015.
11. Gao Y, Siyu Zhang, Zhang X, Du Y, Ni T and Hao S: Crosstalk between metabolic and epigenetic modifications during cell carcinogenesis. iScience 27: 111359, 2024.
12. Lin Y, Li L, Yuan B, Luo F, Zhang X, Yang Y, Luo S, Lin J, Ye T, Zhang Y, *et al*: Phosphorylation determines the glucose metabolism reprogramming and tumor-promoting activity of sine oculis homeobox 1. Signal Transduct Target Ther 9: 337, 2024.
13. Ippolito L, Duatti A, Iozzo M, Comito G, Pardella E, Lorito N, Bacci M, Pranzini E, Santi A, Sandrini G, *et al*: Lactate supports cell-autonomous ECM production to sustain metastatic behavior in prostate cancer. EMBO Rep 25: 3506-3531, 2024.
14. Zhao Y, Liu MJ, Zhang L, Yang Q, Sun QH, Guo JR, Lei XY, He KY, Li JQ, Yang JY, *et al*: High mobility group A1 (HMGA1) promotes the tumorigenesis of colorectal cancer by increasing lipid synthesis. Nat Commun 15: 9909, 2024.
15. Patil K, Johnston E, Novack J, Wallace G, Lin M and Pai SB: Multifaceted impact of HIV inhibitor dapivirine on triple negative breast cancer cells reveals potential entities as targets for novel therapy. Sci Rep 14: 30103, 2024.
16. Lin C, Ye J, Xu C, Zheng Y, Xu Y, Chen Y, Chi L, Lin J, Li F, Lin Y and Wang Q: Evaluating lactate metabolism for prognostic assessment and therapy response prediction in gastric cancer with emphasis on the oncogenic role of SLC5A12. Biochim Biophys Acta Gen Subj 1869: 130739, 2024.
17. Sun D, Lu J, Zhao W, Chen X, Xiao C, Hua F, Hydbring P, Gabazza EC, Tartarone A, Zhao X and Yang W: Construction and validation of a prognostic model based on oxidative stress-related genes in non-small cell lung cancer (NSCLC): Predicting patient outcomes and therapy responses. Transl Lung Cancer Res 13: 3152-3174, 2024.
18. Zhang H, Yang Y, Xing W, Li Y and Zhang S: Expression and gene regulatory network of S100A16 protein in cervical cancer cells based on data mining. BMC Cancer 23: 1124, 2023.
19. Ritchie ME, Phipson B, Wu D, Hu Y, Law CW, Shi W and Smyth GK: Limma powers differential expression analyses for RNA-sequencing and microarray studies. Nucleic Acids Res 43: e47, 2015.
20. Roychowdhury A, Samadder S, Das P, Mazumder DI, Chatterjee A, Addya S, Mondal R, Roy A, Roychoudhury S and Panda CK: Deregulation of H19 is associated with cervical carcinoma. Genomics 112: 961-970, 2020.
21. Fjeldbo CS, Hompland T, Hillestad T, Aarnes EK, Günther CC, Kristensen GB, Malinen E and Lyng H: Combining imaging- and gene-based hypoxia biomarkers in cervical cancer improves prediction of chemoradiotherapy failure independent of intratumour heterogeneity. EBioMedicine 57: 102841, 2020.
22. den Boon JA, Pyeon D, Wang SS, Horswill M, Schiffman M, Sherman M, Zuna RE, Wang Z, Hewitt SM, Pearson R, *et al*: Molecular transitions from papillomavirus infection to cervical precancer and cancer: Role of stromal estrogen receptor signaling. Proc Natl Acad Sci USA 112: E3255-E3264, 2015.
23. Lee YY, Kim TJ, Kim JY, Choi CH, Do IG, Song SY, Sohn I, Jung SH, Bae DS, Lee JW and Kim BG: Genetic profiling to predict recurrence of early cervical cancer. Gynecol Oncol 131: 650-654, 2013.
24. Teschendorff AE, Jones A and Widschwendter M: Stochastic epigenetic outliers can define field defects in cancer. BMC Bioinformatics 17: 178, 2016.
25. Zhai Y, Kuick R, Nan B, Ota I, Weiss SJ, Trimble CL, Fearon ER and Cho KR: Gene expression analysis of preinvasive and invasive cervical squamous cell carcinomas identifies HOXC10 as a key mediator of invasion. Cancer Res 67: 10163-10172, 2007.
26. Leek JT, Johnson WE, Parker HS, Jaffe AE and Storey JD: The sva package for removing batch effects and other unwanted variation in high-throughput experiments. Bioinformatics 28: 882-883, 2012.
27. Cheng Z, Huang H, Li M, Liang X, Tan Y and Chen Y: Lactylation-related gene signature effectively predicts prognosis and treatment responsiveness in hepatocellular carcinoma. Pharmaceuticals 16: 644, 2023.
28. Zhang D, Tang Z, Huang H, Zhou G, Cui C, Weng Y, Liu W, Kim S, Lee S, Perez-Neut M, *et al*: Metabolic regulation of gene expression by histone lactylation. Nature 574: 575-580, 2019.
29. Moreno-Yruela C, Zhang D, Wei W, Bæk M, Liu W, Gao J, Danková D, Nielsen AL, Bolding JE, Yang L, *et al*: Class I histone deacetylases (HDAC1-3) are histone lysine delactylases. Sci Adv 8: eabi6696, 2022.
30. Mariathasan S, Turley SJ, Nickles D, Castiglioni A, Yuen K, Wang Y, Kadel EE III, Koeppen H, Astarita JL, Cubas R, *et al*: TGFβ attenuates tumour response to PD-L1 blockade by contributing to exclusion of T cells. Nature 554: 544-548, 2018.
31. Kurki MI, Karjalainen J, Palta P, Sipilä TP, Kristiansson K, Donner KM, Reeve MP, Laivuori H, Aavikko M, Kaunisto MA, *et al*: FinnGen provides genetic insights from a well-phenotyped isolated population. Nature 613: 508-518, 2023.
32. Stuart T, Butler A, Hoffman P, Hafemeister C, Papalexi E, Mauck WM III, Hao Y, Stoeckius M, Smibert P and Satija R: Comprehensive Integration of Single-Cell Data. Cell 177: 1888-1902.e21, 2019.
33. Korsunsky I, Millard N, Fan J, Slowikowski K, Zhang F, Wei K, Baglaenko Y, Brenner M, Loh PR and Raychaudhuri S: Fast, sensitive and accurate integration of single-cell data with Harmony. Nat Methods 16: 1289-1296, 2019.
34. Jin S, Guerrero-Juarez CF, Zhang L, Chang I, Ramos R, Kuan CH, Myung P, Plikus MV and Nie Q: Inference and analysis of cell-cell communication using CellChat. Nat Commun 12: 1088, 2021.
35. Langfelder P and Horvath S: WGCNA: An R package for weighted correlation network analysis. BMC Bioinformatics 9: 559, 2008.
36. Wyss R, Van Der Laan M, Gruber S, Shi X, Lee H, Dutcher SK, Nelson JC, Toh S, Russo M, Wang SV, *et al*: Targeted learning with an undersmoothed LASSO propensity score model for large-scale covariate adjustment in health-care database studies. Am J Epidemiol 193: 1632-1640, 2024.
37. Binder H and Schumacher M: Allowing for mandatory covariates in boosting estimation of sparse high-dimensional survival models. BMC Bioinformatics 9: 14, 2008.
38. Friedman J, Hastie T and Tibshirani R: Regularization paths for generalized linear models via coordinate descent. J Stat Soft 33: 1-22, 2010.umerical
39. Chen D, Lin D, Li H, Yang J, Liu L, Zhang H, Tang D and Wang K: The glycolytic characteristics of hepatocellular carcinoma and its interaction with the microenvironment: A comprehensive omics study. J Transl Med 23: 424, 2025.
40. Blanche P, Dartigues J and Jacqmin-Gadda H: Estimating and comparing time-dependent areas under receiver operating characteristic curves for censored event times with competing risks. Statistics in Medicine 32: 5381-5397, 2013.
41. Restaino S, Pellecchia G, Arcieri M, Bogani G, Taliento C, Greco P, Driul L, Chiantera V, Ercoli A, Fanfani F, *et al*: Management for cervical cancer patients: A comparison of the guidelines from the international scientific societies (ESGO-NCCN-ASCO-AIOM-FIGO-BGCS-SEOM-ESMO-JSGO). Cancers 16: 2541, 2024.
42. Tang Z, Kang B, Li C, Chen T and Zhang Z: GEPIA2: An enhanced web server for large-scale expression profiling and interactive analysis. Nucleic Acids Res 47: W556-W560, 2019.
43. Subramanian A, Tamayo P, Mootha VK, Mukherjee S, Ebert BL, Gillette MA, Paulovich A, Pomeroy SL, Golub TR, Lander ES and Mesirov JP: Gene set enrichment analysis: A knowledge-based approach for interpreting genome-wide expression profiles. Proc Natl Acad Sci USA 102: 15545-15550, 2005.
44. Hänzelmann S, Castelo R and Guinney J: GSVA: Gene set variation analysis for microarray and RNA-seq data. BMC Bioinf 14: 7, 2013.
45. Yoshihara K, Shahmoradgoli M, Martínez E, Vegesna R, Kim H, Torres-Garcia W, Treviño V, Shen H, Laird PW, Levine DA, *et al*: Inferring tumour purity and stromal and immune cell admixture from expression data. Nat Commun 4: 2612, 2013.
46. Mroz EA and Rocco JW: MATH, a novel measure of intratumor genetic heterogeneity, is high in poor-outcome classes of head and neck squamous cell carcinoma. Oral Oncology 49: 211-215, 2013.
47. Geeleher P, Cox N and Huang RS: pRRophetic: An R package for prediction of clinical chemotherapeutic response from tumor gene expression levels. PLoS One 9: e107468, 2014.
48. Walker VM, Davies NM, Hemani G, Zheng J, Haycock PC, Gaunt TR, Davey Smith G and Martin RM: Using the MR-Base platform to investigate risk factors and drug targets for thousands of phenotypes. Wellcome Open Res 4: 113, 2019.
49. Verbanck M, Chen CY, Neale B and Do R: Detection of widespread horizontal pleiotropy in causal relationships inferred from Mendelian randomization between complex traits and diseases. Nat Genet 50: 693-698, 2018.

50. Cho Y, Haycock PC, Sanderson E, Gaunt TR, Zheng J, Morris AP, Davey Smith G and Hemani G: Exploiting horizontal pleiotropy to search for causal pathways within a mendelian randomization framework. Nat Commun 11: 1010, 2020.
51. Livak KJ and Schmittgen TD: Analysis of relative gene expression data using real-time quantitative PCR and the 2(-Delta Delta C(T)) method. Methods 25: 402-408, 2001.
52. Yordanov A, Damyanova P, Vasileva-Slaveva M, Hasan I, Kostov S and Shivarov V: Integrated analysis of phagocytic and immunomodulatory markers in cervical cancer reveals constellations of potential prognostic relevance. Int J Mol Sci 25: 9117, 2024.
53. Allemani C, Minicozzi P, Morawski B, Lima CA, Bennett D, Pongnikorn D, Petrova D, Innos K, Girardi F, Galán Alvarez Y, *et al*: Global variation in patterns of care and time to initial treatment for breast, cervical, and ovarian cancer from 2015 to 2018 (VENUSCANCER): A secondary analysis of individual records for 275 792 women from 103 population-based cancer registries in 39 countries and territories. Lancet 406: 2325-2348, 2025.
54. Andersen K, Bonde J, Waldstrøm M, Jakobsen MV, Lamy P, Pedersen H, Bønløkke S, Stougaard M and Steiniche T: Evaluation of targeted next-generation sequencing for detection of HPV genotypes and sublineages in cervical liquid-based cytology SurePath samples from the Danish screening program. Int J Cancer 158: 193-201, 2026.
55. Jian X, Cheng C, Lu W, Peng H and Yang D: Histone lactylation: Unveiling a novel pathway for the impact of lactate on physiological and pathological processes (review). Int J Mol Med 57: 1-12, 2025.
56. Dang T, You Y, Wei L, Li Q, Sun H, Sun M, Li X, Yang S, Zeng T, Zhang L, *et al*: ICAT drives lactylation of tumor-associated macrophages via the c-myc-ENO1 axis to promote cervical cancer progression. Free Radic Biol Med 241: 316-329, 2025.
57. Xue ZR, Xin YY and Jin WL: Exploiting metabolic vulnerabilities in cancer: From mechanisms to therapeutic opportunities. Cancer Lett 634: 218067, 2025.
58. Sarwar F, Ashhad S, Vimal A and Vishvakarma R: Small molecule inhibitors of the VEGF and tyrosine kinase for the treatment of cervical cancer. Med Oncol 41: 199, 2024.
59. Mokoala KMG, Lawal IO, Maserumule LC, Bida M, Maes A, Ndlovu H, Reed J, Mahapane J, Davis C, Van de Wiele C, *et al*: Correlation between [68Ga]Ga-FAPI-46 PET imaging and HIF-1α immunohistochemical analysis in cervical cancer: Proof-of-concept. Cancers 15: 3953, 2023.
60. Nasioudis D, Fernandez ML, Wong N, Powell DJ Jr, Mills GB, Westin S, Fader AN, Carey MS and Simpkins F: The spectrum of MAPK-ERK pathway genomic alterations in gynecologic malignancies: Opportunities for novel therapeutic approaches. Gynecol Oncol 177: 86-94, 2023.
61. Del Dotto V, Grillini S, Righetti R, Grandi M, Giorgio V, Solaini G and Baracca A: Bioenergetics of cancer cells: Insights into the warburg effect and regulation of ATP synthase. Mol Med 31: 311, 2025.
62. Wen B, Luo L, Zeng Z and Luo X: MYL9 promotes squamous cervical cancer migration and invasion by enhancing aerobic glycolysis. J Int Med Res 51: 3000605231208582, 2023.
63. Robledo-Cadena DX, Pacheco-Velázquez SC, Vargas-Navarro JL, Padilla-Flores JA, López-Marure R, Pérez-Torres I, Kaambre T, Moreno-Sánchez R and Rodríguez-Enríquez S: Synergistic celecoxib and dimethyl-celecoxib combinations block cervix cancer growth through multiple mechanisms. PLoS One 19: e0308233, 2024.
64. Sheng B, Pan S, Ye M, Liu H, Zhang J, Zhao B, Ji H and Zhu X: Single-cell RNA sequencing of cervical exfoliated cells reveals potential biomarkers and cellular pathogenesis in cervical carcinogenesis. Cell Death Dis 15: 130, 2024.
65. Limones-Gonzalez JE, Aguilar Esquivel P, Vazquez-Santillan K, Castro-Oropeza R, Lizarraga F, Maldonado V, Melendez-Zajgla J, Piña-Sanchez P and Mendoza-Almanza G: Changes in the molecular nodes of the notch and NRF2 pathways in cervical cancer tissues from the precursor stages to invasive carcinoma. Oncol Lett 28: 522, 2024.
66. Hazazi A, Khan FR, Albloui F, Arif S, Abdulaziz O, Alhomrani M, Sindi AAA, Abu-Alghayth MH, Abalkhail A, Nassar SA and Binshaya AS: Signaling pathways in HPV-induced cervical cancer: Exploring the therapeutic promise of RNA modulation. Pathol Res Pract 263: 155612, 2024.
67. Yan Y, Dai T, Guo M, Zhao X, Chen C, Zhou Y, Qin M, Xu L and Zhao J: A review of non-classical MAPK family member, MAPK4: A pivotal player in cancer development and therapeutic intervention. Int J Biol Macromol 271: 132686, 2024.
68. Zheng X, Tong T, Duan L, Ma Y, Lan Y, Shao Y, Liu H, Chen W, Yang T and Yang L: VSIG4 induces the immunosuppressive microenvironment by promoting the infiltration of M2 macrophage and Tregs in clear cell renal cell carcinoma. Int Immunopharmacol 142: 113105, 2024.
69. Miao C, You X, Zhang Z, Jiang Z, Liu L, Jia Y, Bai J, Gao Y, Ye L, Cao Y, *et al*: SCG2 mediates HNSCC progression with CCL2/TGFβ1 M2 macrophage infiltration. Oral Dis 31: 782-795.
70. Feng L, Shi Q, Wang S, Zhao Y, Wu H, Wei L, Hao Q, Cui Z, Wang L, Zhang J, *et al*: The outcome of advanced and recurrent cervical cancer patients treated with First-line platinum and paclitaxel with or without indication for immune checkpoint inhibitors: The comparative study. BMC Cancer 24: 1267, 2024.